Chemical Engineering Journal 427 (2022) 131578

Contents lists available at ScienceDirect

Chemical Engineering Journal

journal homepage: www.elsevier.com/locate/cej

Flame-retardant, transparent, mechanically-strong and tough epoxy resin enabled by high-efficiency multifunctional boron-based polyphosphonamide

Siqi Huo [a,b,*], Zhongxiao Zhou [a], Jiawei Jiang [c], Ting Sai [a,b], Shiya Ran [a], Zhengping Fang [a,b,*], Pingan Song [d], Hao Wang [d]

[a] Laboratory of Polymer Materials and Engineering, NingboTech University, Ningbo 315100, China
[b] MOE Key Laboratory of Macromolecular Synthesis and Functionalization, Department of Polymer Science and Engineering, Zhejiang University, Hangzhou 310027, China
[c] College of Chemical and Biological Engineering, Zhejiang University, Hangzhou 310027, China
[d] Centre for Future Materials, University of Southern Queensland, Toowoomba, QLD 4350, Australia

ARTICLE INFO

Keywords:
Epoxy resin
Boron-derived polyphosphonamide
Flame retardancy
Thermal stability
Mechanical properties

ABSTRACT

It is of great significance to develop high-performance epoxy resins (EPs) combining superior flame retardancy, smoke suppression, thermal oxidation stability, transparency and mechanical properties. However, current flame retardant design strategy usually realizes satisfied flame retardancy at the expense of other properties. Herein, a novel multifunctional high-efficiency boron-containing polyphosphonamide (PB) is synthesized, and its impacts on integrated properties of EP are studied thoroughly. As expected, the well-designed PB features high flame retardant efficiency due to the combination of phosphorus, boron and nitrogen elements, only 3 wt% of which increases the limiting oxygen index (LOI) and UL-94 classification of EP thermoset to 32.2% and V-0, with a ~32.2% decrease in the peak smoke production rate (PSPR). Compared with the unmodified EP sample, the tensile strength, elongation at break and impact strength of EP sample with 3 wt% PB are elevated by ~29.8%, ~37.7% and ~50.2%, respectively. Meanwhile, high glass transmission temperature and transparency are maintained. Hence, this work offers an integrated strategy to develop highly efficient multifunctional polyphosphonamides for the preparation of high-performance flame-retardant and smoke-suppressive EPs combining high mechanical strength and toughness, thermal resistance and transparency, which are expected to meet the increasingly rigorous industrial requirements.

1. Introduction

Polymeric materials have penetrated into every aspect of our life due to their light weight, low cost, superior chemical resistance, electric insulation and mechanical performances [1–4]. As is well known, fire is one common disaster that poses a serious threat to the public safety and brings great loss of mankind annually, and unfortunately most of polymeric materials are highly flammable, thus the fire-proof requirements on them are continuously raising in recent years [5–7]. Although epoxy resins (EPs), as one of the most common polymers, exhibit outstanding integrated performances, they also suffer from inflammability, e.g., low limiting oxygen index (LOI) of 23–26% and no rating (NR) in UL-94 vertical burning test [8–10]. Hence, it is of great significance to address the flammability issues of EPs. Traditionally, halogen-based flame retardants (FRs) are able to impart great flame retardancy to epoxy resins, but they will release a great deal of toxic and harmful smoke during combustion, thus many of them have been prohibited [11–14]. This has significantly driven the development of halogen-free alternatives for epoxy resins.

Phosphorus (P)-based FRs have been recognized as one of the most promising halogen-free FRs for their good thermal stability and low toxicity/smoke [15–17]. P-based FRs can be simply divided into two types: low-molecular and oligomeric/polymeric [18–20]. Generally, the low-molecular P-based FRs enhance the flame retardancy of EPs at the expense of mechanical properties, e.g., strength and toughness, and they face the migration and leaching issues during practical applications. By

* Corresponding authors at: Laboratory of Polymer Materials and Engineering, NingboTech University, Ningbo 315100, China.
E-mail addresses: sqhuo@nbt.edu.cn (S. Huo), zpfang@nbt.edu.cn (Z. Fang).

https://doi.org/10.1016/j.cej.2021.131578
Received 10 May 2021; Received in revised form 30 June 2021; Accepted 25 July 2021
Available online 10 August 2021

contrast, the oligomeric/polymeric P-based FRs can effectively avoid these issues, and some of them can even improve the flame retardancy and mechanical properties simultaneously [18,21,22]. For instance, Wang et al. [23] synthesized a 9, 10-dihydro-9-oxa-10-phosphaphenanthrene 10-oxide (DOPO)-derived oligomer (PDAP) for the preparation of flame-retardant epoxy resins. With the addition of 7 wt% of PDAP, the as-prepared EP sample exhibits a high LOI of 35.3% with a UL-94 V-0 rating. Meanwhile, its tensile strength is increased from 74.16 MPa of the neat EP sample to 82.44 MPa by 11.2%. Wang et al. [24] reported the synthesis of a poly(DOPO substituted phenyl dimethanol pentaerythritol diphosphonate) (PFR) by polycondensation of DOPO-disubstituted benzenedimethanol with pentaerythritol diphosphonate dichloride. 15 wt% of PFR endows epoxy thermoset with enhanced flame retardancy and toughness, e.g., a high LOI of 36.0%, a UL-94 V-0 rating, a 60% reduction in peak heat release rate (PHRR, obtained from microscale combustion calorimeter) and a 50% increase in elongation at break. Zhang et al. [25] also reported a multifunctional P-containing hyperbranched flame retardant (ITA-HBP) for EPs, which combined the flame-retardant, reinforcing and toughening effects. These attempts have indicated that the application of oligomeric/polymeric P-containing flame retardants is able to maintain the inherent mechanical properties of epoxy thermosets.

Unfortunately, the low flame-retardant efficiency is one major issue of oligomeric/polymeric P-containing flame retardants, leading to a high loading level (>5 wt%) required to achieve satisfactory flame retardancy (e.g., a UL-94 V-0 rating). In previous works, it had been proved that introducing additional flame-retardant atoms, such as boron (B), silicon (Si) and nitrogen (N), into P-based FRs contributed to boosting the flame-retardant efficiency [26–29]. For example, Qiu et al. [30] reported a P/N-containing high-efficiency flame retardant (TOD) for epoxy resin. 4 wt% of TOD increases the LOI and UL-94 classification of EP thermoset to 35.9% and V-0, with 42.4% and 46.5% reductions in PHRR and total heat release (THR). Similar P/N-containing flame retardant for epoxy resin has also been reported in other works [31–33]. Additionally, Duan et al. [34] synthesized a P/N/B-containing flame retardant (TDB) *via* substitution and esterification between 1,3,5-tris(2-

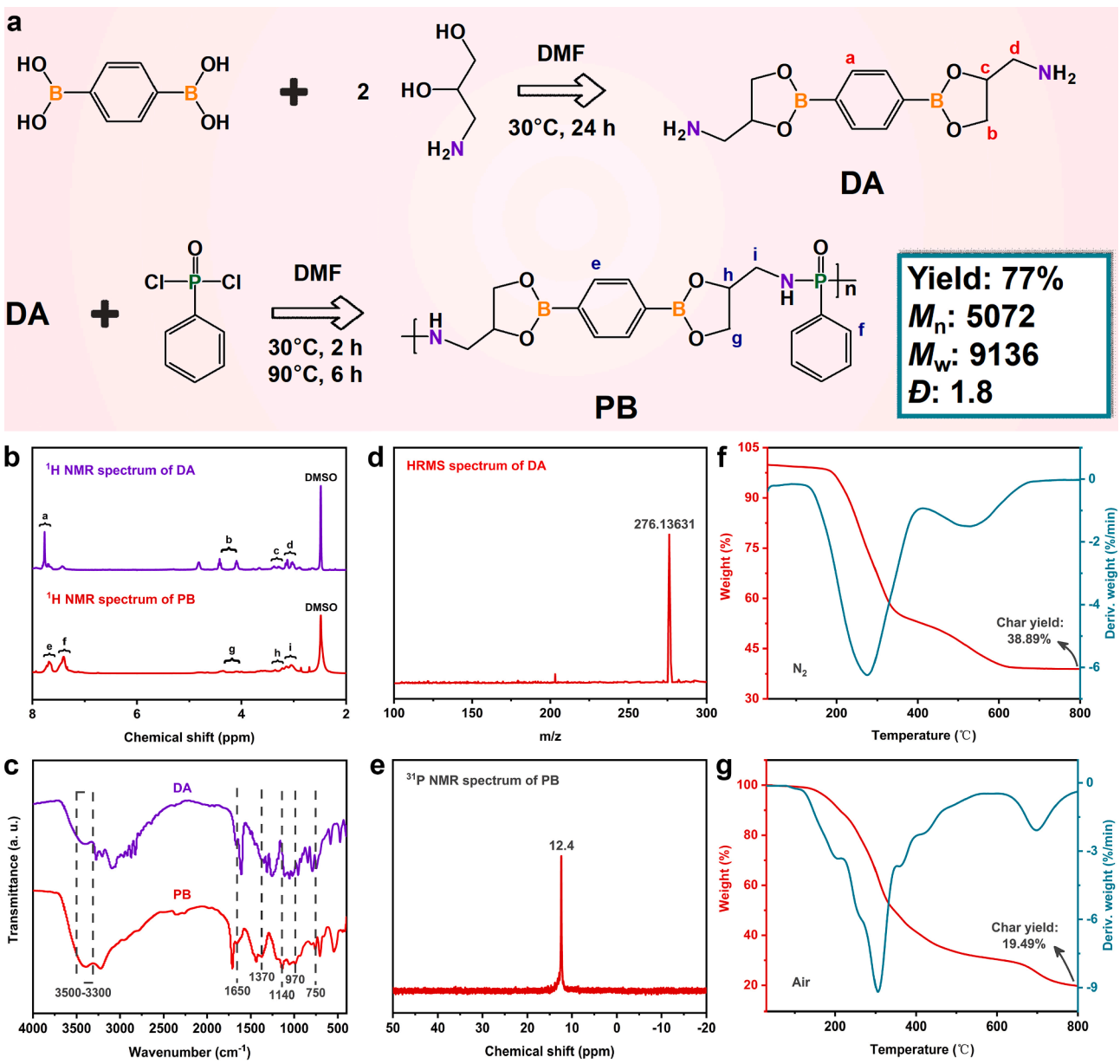

Fig. 1. (a) Synthetic route of PB, (b) ^{1}H NMR spectra of DA and PB, (c) FTIR spectra of DA and PB, (d) HRMS spectrum of DA, (e) ^{31}P NMR spectrum of PB, TG and DTG curves of PB in (f) N_2 and (g) air conditions.

hydroxyethyl)isocyanurate, diphenyl phosphoryl chloride and boric acid. Compared with the neat EP sample, EP composite with 10 wt% TDB shows 52.7%, 30.4%, and 29.2% decreases in PHRR, THR and total smoke production (TSP), demonstrating obviously improved flame retardancy and smoke suppression. Accordingly, the efficiency of P-based FRs can be increased *via* introducing other flame-retardant elements, and thus integrating multiple flame-retardant elements into oligomeric/polymeric FRs may be an effective strategy for creating multifunctional high-efficiency flame retardants. However, such multi-flame-retardant-element oligomers/polymers for epoxy resins are rarely reported.

Herein, this work aims to develop a highly efficient oligomeric P-containing FR (PB) with multiple efficacies *via* introducing boron into polyphosphonamide, which is employed for the fabrication of high-performance epoxy resin. Our results show that only 3 wt% of PB raises the LOI and UL-94 classification of EP thermoset to 32.2% and V-0, and decreases the PHRR and PSPR by ~24.6% and ~32.2% due to the synergistic effect of P, N and B atoms. Notably, EP thermoset with 3 wt% PB exhibits improved mechanical strength and toughness, of which the tensile strength, elongation at break and impact strength are increased by ~29.8%, ~37.7% and ~50.2%, respectively, reflecting the reinforcing and toughening effects of PB. Besides, this EP thermoset shows high glass transition temperature (180 °C) and transmittance (76.3%). This work provides a rational design for creating multifunctional high-efficiency oligomeric flame retardants to fabricate thermally-resistant, transparent, mechanically-strong/tough, flame-retardant and smoke-suppressive EPs, which are expected to find extensive applications in many industrial fields.

2. Experimental section

2.1. Materials

Bisphenol-A type epoxy resin (DGEBA, epoxy value: 0.53 mol/100 g) was obtained from Yueyang Baling Huaxing Petrochemical Co., Ltd. (Hunan, China). 1,4-Phenylenebisboronic acid, 3-amino-1,2-propanediol, phenylphosphonic dichloride, *N*,*N*'-dimethylformamide (DMF), ethanol (EtOH) and 30% ammonium hydroxide solution were purchased from Energy Chemical Co., Ltd. (Shanghai, China). 4,4′-Diaminodiphenyl methane (DDM) was provided by Sinopharm Chemical Reagent Co., Ltd. (Shanghai, China). Deionized water was made by our laboratory. All chemicals were employed as received.

2.2. Synthesis of boron (B)-containing compound (DA)

The synthetic procedure of the intermediate product (DA) is presented in Fig. 1a. Firstly, 9.895 g of 3-amino-1,2-propanediol, 150 mL DMF and 0.3 g of deionized water were introduced into a single-neck flask equipped with a magnetic stirrer. After stirring for 10 min, a transparent solution was obtained, and 9 g of 1,4-phenylenebisboronic acid was added in batches within 2 h at room temperature. Then, the mixture was continuously stirred for 24 h. Then, the crude products were obtained by filtration, followed by washing with DMF for 2–3 times and vacuum-dried for 24 h at 120 °C. The yield of the obtained intermediate product (DA) was 72%. In addition to the synthesis of PB, DA was also applied as a control flame retardant.

2.3. Synthesis of boron (B)-containing polyphosphonamide (PB)

3.0 g of DA and 40 mL DMF were mixed for 30 min in a dried three-neck flask equipped with a mechanical stirrer, dropping funnel, reflux condenser and nitrogen inlet. 1.9 g of phenylphosphonic dichloride dissolved in 20 mL DMF was added dropwise to the flask for 2 h at room temperature. Afterwards, the mixture was heated to 90 °C and stirred for 6 h, and the evolved hydrogen chloride was taken away by nitrogen flow. The mixture was cooled down to room temperature, and then it was filtered. The filtrate was evaporated under reduced pressure at 90 °C and the final product (PB) was obtained after vacuum-drying at 120 °C for 24 h with a yield of 78%. The synthesis route was also presented in Fig. 1a.

2.4. Synthesis of phenylphosphonic diamine (PD)

Phenylphosphonic diamine (PD) was synthesized successfully according to previous work [35], which was utilized as another control flame retardant to investigate the synergistic flame retardant effect between boron-containing and phosphorus-containing groups in PB. The ^{1}H and ^{31}P nuclear magnetic resonance (NMR) spectra of PD were presented in Fig. S1.

2.5. Fabrication of EP thermosets

The flame retardant EP samples containing 1, 2, 3 and 5 wt% of PB were prepared using DDM as curing agent, and denoted as EP/DDM/PB-1, EP/DDM/PB-2, EP/DDM/PB-3 and EP/DDM/PB-5. Besides, the neat EP and EP thermosets containing 3 wt% DA or PD were fabricated as control samples, and named as EP/DDM, EP/DDM/DA-3 and EP/DDM/PD-3. The detailed preparation procedure was as follows, with the formulations listed in Table S1. Typically, PB and EtOH (1 g PB : 10 mL EtOH) were added into a flask and a transparent solution was obtained *via* ultrasonication for 30 min. DGEBA was introduced, and the solution was stirred for 2 h at 80 °C to remove EtOH. Then, DDM was added, and the mixture was stirred for 15 min to become transparent. After debubbling for 5 min under vacuum, the solution was casted into a preheated mould and respectively curing at 120 °C, 140 °C, 160 °C and 180 °C for 2 h, followed by cooling down to room temperature to obtain transparent sample. EP/DDM/DA-3 and EP/DDM/PD-3 were prepared *via* the same process. EP/DDM was fabricated by directly mixing DGEBA and DDM at 80 °C and curing at the temperature programming mentioned above.

2.6. Characterizations

^{1}H and ^{31}P nuclear magnetic resonance (NMR) spectra were collected *via* DD2 400-MR spectrometer (Agilent, USA), with the solvent of DMSO-d_6. Fourier transform infrared (FTIR) spectra were obtained from Nicolet 6700 spectrometer (Thermo Fisher Scientific, USA) in wavenumber range of 400–4000 cm^{-1} using KBr pellet. High-resolution mass spectroscopy (HRMS) was performed on Bruker solanX 70 FT-MS (Bruker, USA). The number-average molecular weight (M_n), weight-average molecular weight (M_w) and dispersity ($Đ$) of PB were tested using gel permeation chromatography (PL-GPC50, Aligent, USA), with the solvent of DMF and the standard of polystyrene. Thermogravimetric analysis (TGA) was conducted on TGA 209 F1 thermogravimetric analyzer (Netzsch, Germany) from 30 °C to 800 °C using a heating rate of 20 °C/min in air or N_2 condition.

Dynamic mechanical analysis (DMA) was carried out on DMA Q800 apparatus (TA Instruments, USA) under single cantilever bending mode at a heat-up rate of 3.00 °C/min from 30 °C to 250 °C. The tensile properties were investigated *via* SHK-A104 universal electronic instrument (Hengke, China) at a stretch speed of 5 mm/min according to the standard of GB/T 1040.1–2006. Five specimens were tested for each sample. Notched Izod impact strength was tested on ZBC1400-B Izod impact equipment (Xinsansi, China) based on ISO180/179 standard, with the specimen dimension of 80 mm × 10 mm × 4 mm and the notch depth of 2 mm. The result was the averaged of five specimens.

The transparency of EP samples was evaluated by WGT-S transmittance/haze tester (Shanghai ShenGuang Instrument Co, China), with the film thickness of 0.3 mm. The result was the average of five different positions in one film. The UV–Vis spectra of EP thin films were recorded on Lambda 35 spectrophotometer (PerkinElmer, USA) in the visible region (wavelength: 400–800 nm). X-ray diffraction (XRD) of EP

samples was conducted on X-ray diffractometer (X'Pert PRO MPD, Holland) with Cu Kα radiation (λ = 1.542 Å) source.

Limiting oxygen index (LOI) was recorded *via* PX-01-005 oxygen index instrument (Phinix, China) based on ASTM D2863, and the specimen dimension was 130 × 6.5 × 3 mm^3. The UL-94 rating was measured on CZF-3 vertical combustion tester (Jiangning, China) according to ISO-1210, with the specimen dimension of 130 × 13 × 3 mm^3. Cone calorimeter test was conducted on FTT-0242 cone calorimeter (Fire Testing Technology, UK) in accordance with ISO 5660 under an external flux of 50 kW/m^2. The sample dimension was 100 × 100 × 3.0 mm^3. The results listed in this work were the averages of three specimens.

The microstructures of char residues for EP samples after cone calorimeter test and fracture surfaces of EP samples after impact test were observed by scanning electron microscope (SEM, JSW-5510LV, EOL, Japan). The chemical compositions of residual chars were investigated *via* ESCALAB XI + X-ray photoelectron (XPS) spectrometer (Thermo Fisher Scientific, USA) with Al Kα radiation. Real-time Fourier transform infrared (RT-FTIR) spectrophotometer (Nicole IN 10, Thermo Fisher Scientific, USA) was employed to investigate the evolved char residues of EP thermosets during thermal oxidation degradation, which was equipped with a heating device. The KBr pellet technique was used

Table 1
The characteristic data of thermal stability of EP thermosets.

Condition	Sample	$T_{5\%}$ (°C)	T_{max1} (°C)	T_{max2} (°C)	Char yield (%)	
					Calculated value	Experimental value
N_2	EP/DDM	371	400	/	/	16.25
	EP/DDM/DA-3	371	402	/	16.51	20.81
	EP/DDM/PD-3	360	403	/	16.20	18.17
	EP/DDM/PB-1	370	405	/	16.48	18.76
	EP/DDM/PB-2	351	403	/	16.70	18.81
	EP/DDM/PB-3	347	402	/	16.93	19.86
	EP/DDM/PB-5	329	400	/	17.38	20.04
Air	EP/DDM	271	287	532	/	0.95
	EP/DDM/DA-3	270	299	532	1.51	0.33
	EP/DDM/PD-3	276	290	538	1.03	1.75
	EP/DDM/PB-1	270	289	535	1.14	1.60
	EP/DDM/PB-2	276	299	539	1.32	1.63
	EP/DDM/PB-3	279	290	534	1.51	1.68
	EP/DDM/PB-5	272	293	534	1.88	3.15

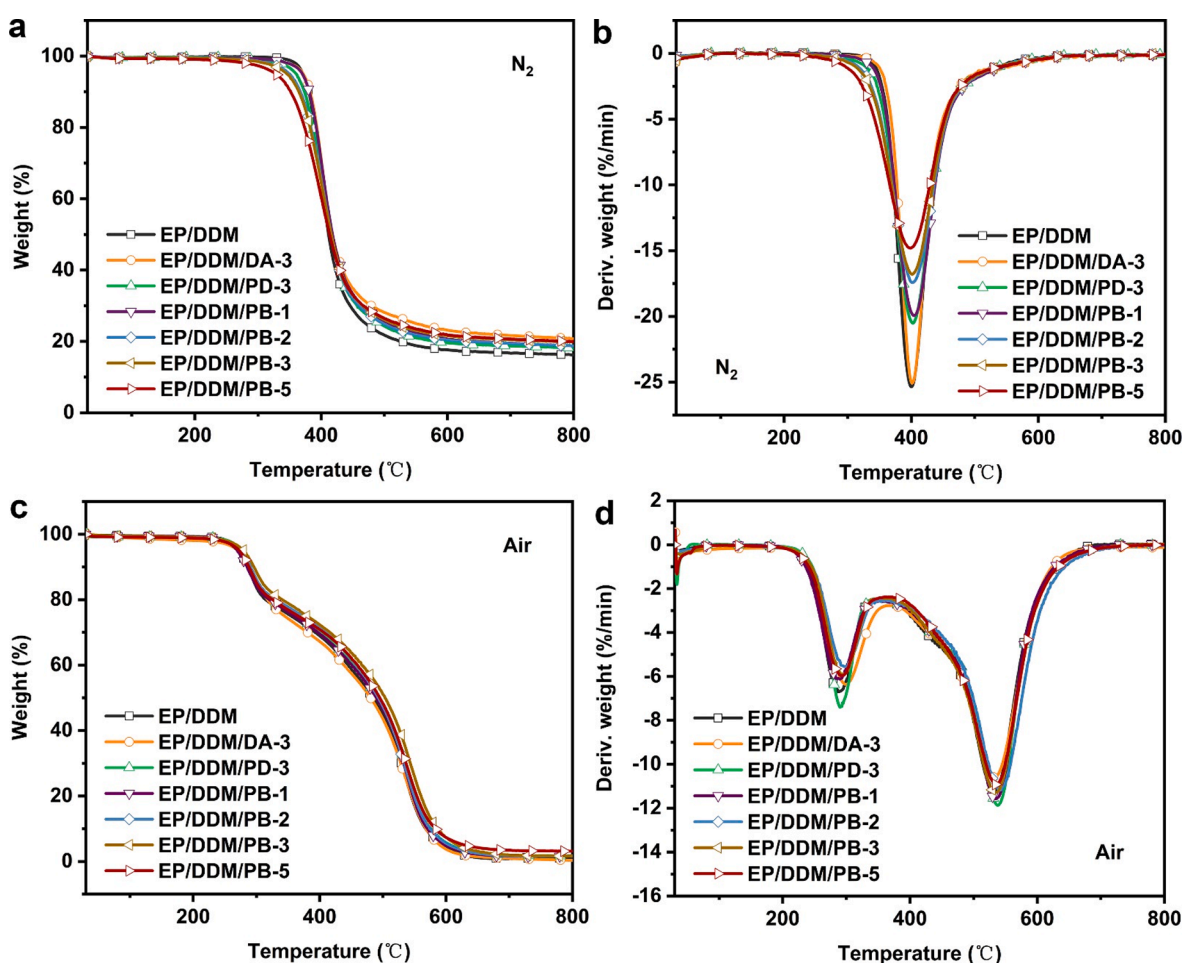

Fig. 2. TG and DTG curves of EP thermosets under (a, b) N_2 and (c, d) air flows.

and heat-up rate was 10 °C/min.

The gaseous decomposition products of EP samples were investigated by TGA coupled with FT-IR (TG-IR, Thermo-Nicolet iS-10). Acquisition interval was 2.24 s with the resolution of 4 cm^{-1}. To study the pyrolysis behaviors of EP samples, pyrolysis–gas chromatography-mass spectrometry (py-GC–MS) analysis was performed on Agilent 7890/5975 GC/MS. The GC/MS interface and cracker temperatures were set to 280 °C and 500 °C, respectively.

3. Results and discussion

3.1. Synthesis and characterization of PB

The synthesis of B-containing polyphosphonamide (PB) is composed of two steps (see Fig. 1a). The first step is the fabrication of the intermediate product (DA) *via* the dehydration reaction between 3-amino-1,2-propanediol and 1,4-phenylenebisboronic acid. The second step is the elimination reaction of DA and phenylphosphonic dichloride.

The molecular structure of DA is respectively characterized by FTIR, ^{1}H NMR and HRMS measurements, with the spectra shown in Fig. 1b–d. As shown in the ^{1}H NMR spectrum of DA, the signal at about 7.8 ppm belongs to the protons of benzene group. The chemical shifts at 4.4 and 4.1 ppm are attributed to the protons of methylene in cyclic borate, and those at 3.2–3.5 ppm are assigned to the protons of methyne. Besides, the signals at 3.0–3.2 ppm are ascribed to the protons of methylene attached to amino. The integral area ratio of a, b, c and d peaks is 4: 3.89: 1.96: 3.94, which is very close to the theoretical ratio of the corresponding protons in DA. As presented in the FTIR spectrum of DA, the absorption bands of N-H appear at 3300–3500 cm^{-1} [36]; the stretching vibration of the aromatic ring centers at 1650 cm^{-1} [37]; the absorption peak of B-O-C appears at 1370 cm^{-1} [38]. Meanwhile, the m/z of DA is 276.13631 $[M+H]^+$, which is consistent with the theoretical molecular weight of DA (see Fig. 1d). All these results confirm that the boron-based intermediate product (DA) has been successfully synthesized.

The chemical structure of PB is identified by NMR, FTIR and GPC techniques, and the spectra are presented in Fig. 1**b–e**. Besides the

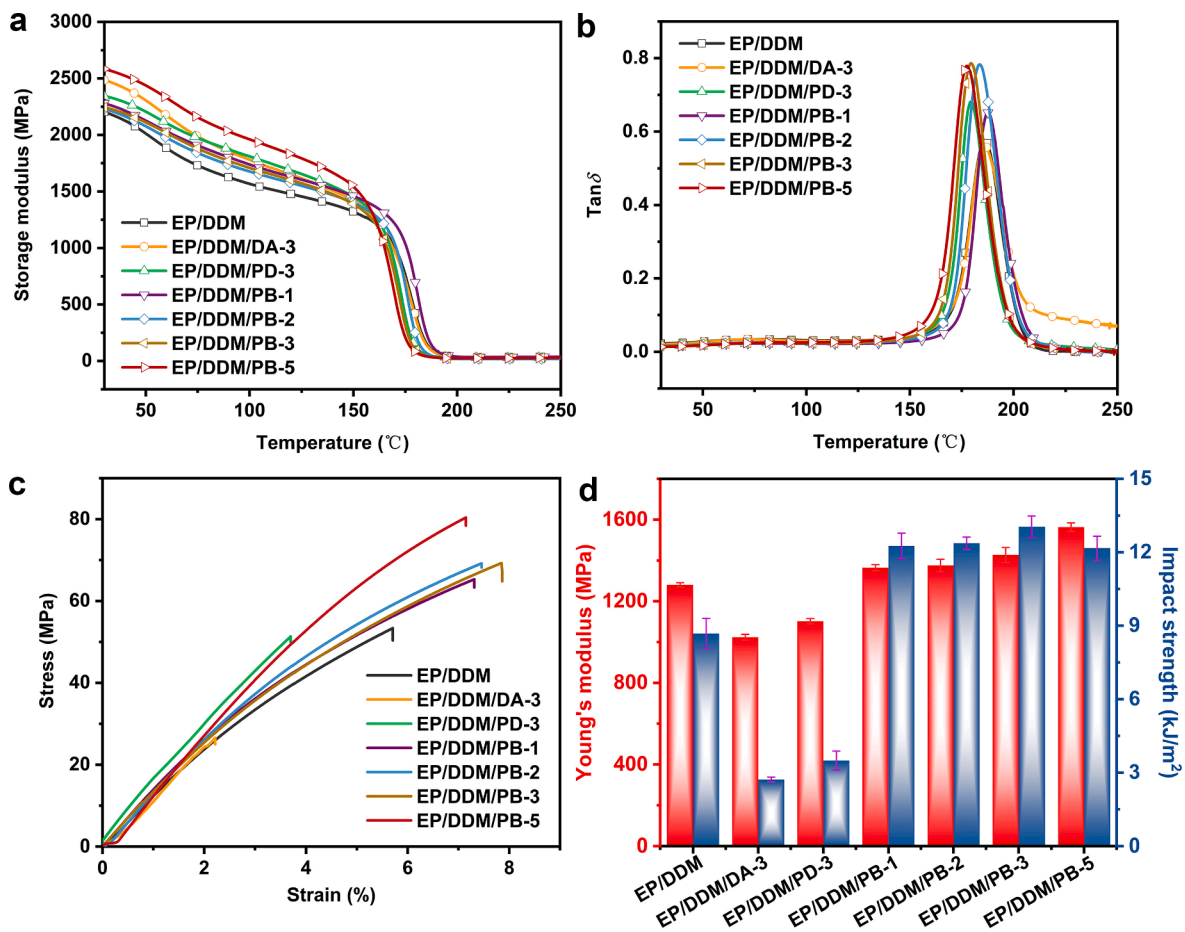

Fig. 3. (a) Storage modulus plots, (b) Tanδ, (c) stress–strain curves and (d) Young's moduli and impact strengths of EP thermosets.

Table 2
Data of EP thermosets obtained from DMA, tensile and impact tests.

Sample	T_g [a] (°C)	E' [a] (MPa)	Tensile strength (MPa)	Young's modulus (MPa)	Elongation at break (%)	Impact strength (kJ/m^2)
EP/DDM	186	2204	53.4 ± 3.0	1280.2 ± 10.5	5.7 ± 0.5	8.7 ± 0.6
EP/DDM/DA-3	186	2486	22.6 ± 1.7	1023.9 ± 14.3	2.2 ± 0.7	2.7 ± 0.1
EP/DDM/PD-3	179	2343	51.9 ± 2.5	1102.3 ± 12.8	3.7 ± 0.7	3.5 ± 0.4
EP/DDM/PB-1	187	2280	65.3 ± 3.2	1364.5 ± 15.1	7.3 ± 0.6	12.3 ± 0.5
EP/DDM/PB-2	184	2231	69.2 ± 1.6	1375.4 ± 30.5	7.5 ± 0.3	12.4 ± 0.3
EP/DDM/PB-3	180	2245	69.3 ± 1.6	1426.9 ± 36.4	7.9 ± 0.3	13.0 ± 0.4
EP/DDM/PB-5	177	2584	80.4 ± 2.7	1563.4 ± 20.9	7.1 ± 0.5	12.2 ± 0.5

[a] T_g: glass-transition temperature, and E': storage modulus at 30 °C.

signals of DA mentioned above, PB also exhibits the chemical shift at ~7.4 ppm, belonging to the phenyl in phenylphosphonic group (see Fig. 1b). Meanwhile, there are some new characteristic peaks can be observed in the FTIR spectrum of PB (see Fig. 1c). In detail, the newly emerging absorption peaks at 1140, 970 and 750 cm^{-1} are assigned to P═O, P—N and P—C, respectively [39,40]. As presented in Fig. 1e, there is only one peak at 12.4 ppm in the ^{31}P NMR spectrum of PB, which is attributed to the phosphorus atom in phenylphosphonic group. According to GPC result, the number-average molecular weight (M_n) and dispersity ($Đ$) of PB are 5072 and 1.8, respectively, demonstrating its polyphosphonamide structure. Such results verify the successful fabrication of B-based polyphosphonamide (PB).

The thermal stability of PB in nitrogen or air condition is investigated by TGA, with the curves shown in Fig. 1f and g. In addition, the TG and DTG curves of the control flame retardants (DA and PD) are shown in Fig. S2. The initial decomposition temperature ($T_{5\%}$, the temperatures at 5% weight loss) of PB are around 205 °C, which may be attributed to the release of H_2O, and such $T_{5\%}$ is higher than the curing temperature of EP/DDM system (120–180 °C), meaning that PB can meet the solidification requirement. In addition, PB exhibits the maximum mass loss temperatures (T_{max}s) of ~300 °C in both nitrogen and air conditions, which are lower than the $T_{5\%}$s of EP/DDM (see Table 1), demonstrating that PB can thermally degrade to form a protective char shield before the decomposition of EP matrix. Meanwhile, the char yields of PB reach 38.89% and 19.49% under N_2 and air flows, respectively, which are much higher than those of DA and PD, indicating its superior high-temperature stability and carbonization capacity due to the combination of N, B and P atoms. Such results demonstrate that the as-synthesized PB can serve as an ideal flame retardant for epoxy thermoset due to its relatively low decomposition temperature and superior carbonization capacity.

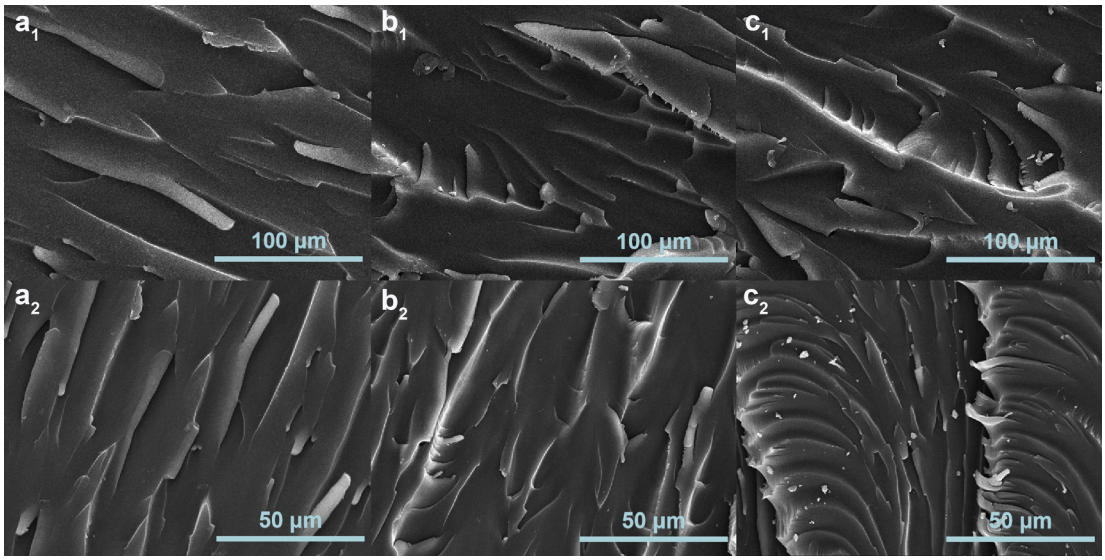

Fig. 4. SEM micrographs of Izod impact fractured surfaces of (a_1, a_2) EP/DDM, (b_1, b_2) EP/DDM/PB-3, and (c_1, c_2) EP/DDM/PB-5 under different magnifications.

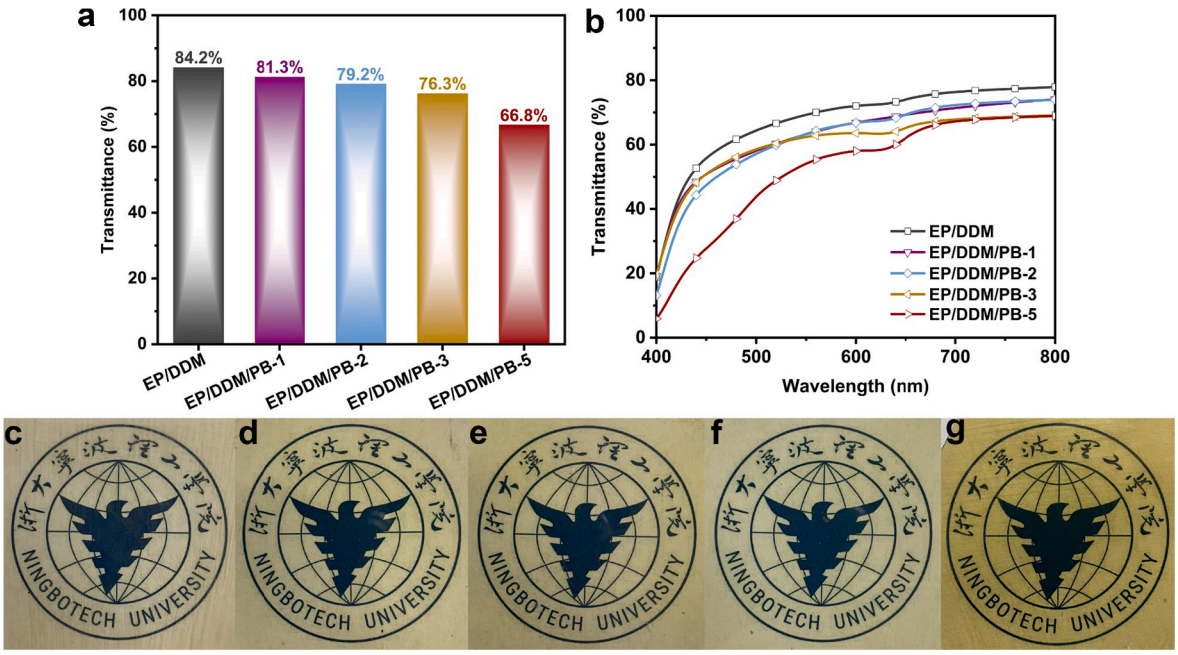

Fig. 5. (a) Transmittance of EP samples, (b) UV–Vis spectra curves of EP samples in visible region, and digital photos of (c) EP/DDM, (d) EP/DDM/PB-1, (e) EP/DDM/PB-2, (f) EP/DDM/PB-3 and (g) EP/DDM/PB-5 samples.

3.2. Thermal stability of EP thermosets

The TG and DTG curves of EP thermosets are presented in Fig. 2, with the characteristic data ($T_{5\%}$, T_{max1}, T_{max2} and char yield) listed in Table 1. In N_2 condition, EP/DDM shows a single-step decomposition, with a $T_{5\%}$ of 371 °C, a T_{max1} of 400 °C and a char yield of 16.25%. The decomposition procedure of EP/DDM involves the breakage of C—O, C—N, hydrocarbons and aromatic ring [41,42]. With the introduction of PB, the $T_{5\%}$s of EP/DDM/PB samples are gradually reduced, but they are all above 320 °C, manifesting relatively high initial decomposition temperatures. Notably, the T_{max1}s of EP/DDM/PB samples (400–405 °C) are the same as and even higher than that of EP/DDM (400 °C). Such results demonstrate that PB decomposes in advance to form thermally-stable char to retard the degradation of epoxy matrix. Based on the char yields of PB and EP/DDM, the theoretical char yields of EP/DDM/PB samples are calculated, with the values listed in Table 1. All EP/DDM/PB samples exhibit higher experimental char yields than the calculated ones, indicating the promotion effect of PB on the char formation of the epoxy matrix. Similar results can be observed in the char yields of EP/DDM/DA-3 and EP/DDM/PD-3 thermosets, which demonstrates that both of them can facilitate the carbonization of EP/DDM. Thus, PB combining superior high-temperature stability and promoting char-formation effect can not only suppress the thermal decomposition but also facilitate the charring of EP matrix.

Under air flow, EP shows two degradation steps. In detail, the first stage is attributed to the degradation of EP skeleton, and the second one is ascribed to the thermal oxidation decomposition of char residues [17]. Interestingly, the $T_{5\%}$, T_{max1}, and T_{max2} of EP/DDM/PB thermosets are all higher than those of EP/DDM thermoset, demonstrating that PB enhances the thermo-oxidative stability of EP/DDM/PB thermosets. The promotion effect of PB on char formation can also be confirmed by the difference between the experimental and calculated char yields in air condition. All these results manifest that PB is capable of suppressing the decomposition and promoting the charring formation of EP matrix in both N_2 and air conditions.

3.3. Dynamic and static mechanical properties of EP thermosets

The impacts of PB, DA and PD on the dynamic and static mechanical properties of EP thermosets are investigated by DMA, tensile and notched Izod impact tests, with the results shown in Fig. 3 and Table 2. The neat EP/DDM sample exhibits a high T_g of 186 °C, with a E' of 2204 MPa (see Table 2). Incorporating PB leads to a reduction in T_g, followed by an increase in E'. For instance, the T_gs of EP/DDM/PB-3 and EP/DDM/PB-5 samples decrease to 180 °C and 177 °C, while the E's increase to 2245 and 2584 MPa. It is supposed that some epoxy groups in

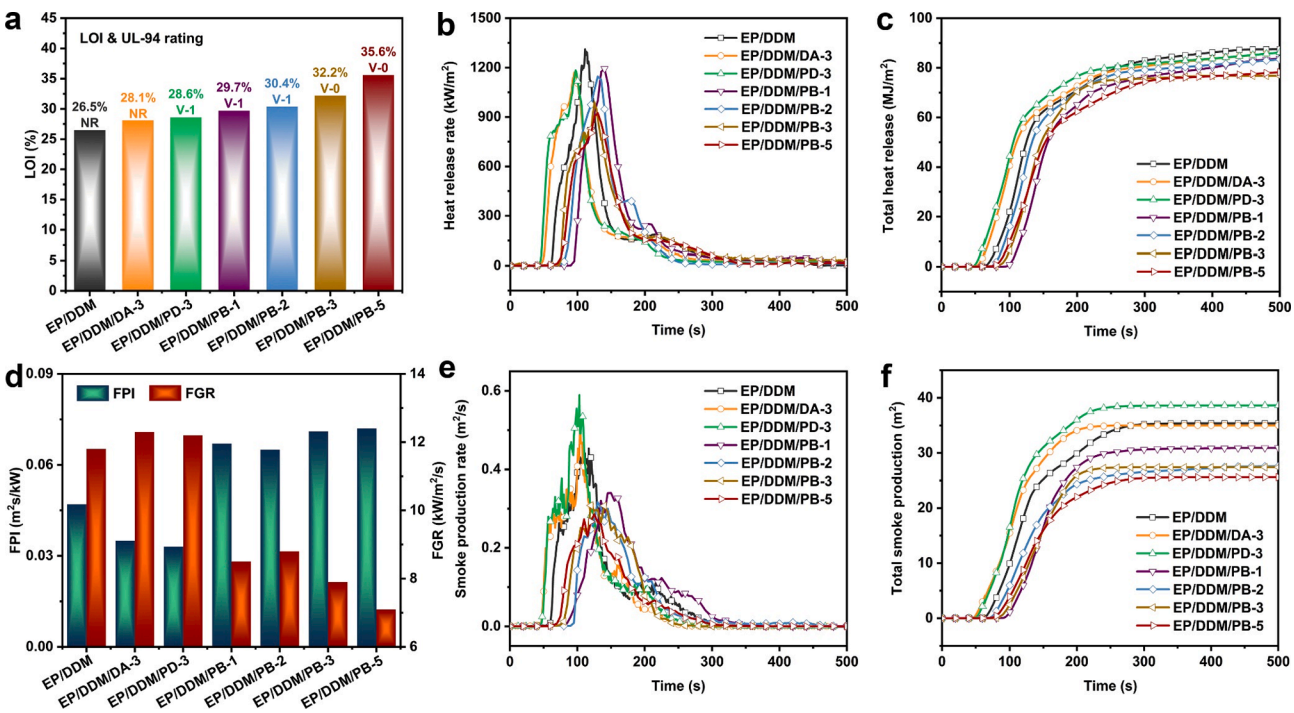

Fig. 6. (a) LOI values and UL-94 ratings, (b) heat release rate curves, (c) total heat release plots, (d) fire performance indexes and fire growth rates, (e) smoke production rate curves, and (f) total smoke production plots of EP samples.

Table 3
Data obtained from cone calorimeter tests of EP samples.

Sample code	TTI[a] (s)	PHRR[a] (kW/m²)	THR[a] (MJ/m²)	FPI[a] (m²s/kW)	FGR[a] (kW/m²/s)	PSPR[a] (m²/s)	TSP[a] (m²)	AEHC[a] (MJ/kg)	RW[a] (%)
EP/DDM	62 ± 3	1311 ± 61	87.5 ± 4.1	0.047 ± 0.003	11.8 ± 0.6	0.453 ± 0.022	35.4 ± 2.0	24.4 ± 1.2	10.3 ± 0.5
EP/DDM/DA-3	41 ± 2	1171 ± 56	85.9 ± 4.2	0.035 ± 0.002	12.3 ± 0.5	0.537 ± 0.025	35.0 ± 1.8	23.8 ± 1.2	14.9 ± 0.7
EP/DDM/PD-3	39 ± 2	1184 ± 57	86.2 ± 3.8	0.033 ± 0.002	12.2 ± 0.5	0.589 ± 0.030	38.6 ± 2.2	23.5 ± 1.0	12.4 ± 0.6
EP/DDM/PB-1	80 ± 4	1193 ± 54	83.7 ± 3.9	0.067 ± 0.004	8.5 ± 0.3	0.340 ± 0.017	30.9 ± 1.5	23.8 ± 1.3	13.1 ± 0.7
EP/DDM/PB-2	74 ± 3	1146 ± 48	83.3 ± 3.7	0.065 ± 0.003	8.8 ± 0.2	0.317 ± 0.022	27.6 ± 1.3	23.5 ± 1.1	16.1 ± 0.8
EP/DDM/PB-3	70 ± 2	989 ± 45	76.7 ± 4.0	0.071 ± 0.003	7.9 ± 0.3	0.307 ± 0.019	27.4 ± 1.4	23.5 ± 1.3	16.3 ± 0.8
EP/DDM/PB-5	66 ± 3	923 ± 46	78.2 ± 3.6	0.072 ± 0.004	7.1 ± 0.3	0.286 ± 0.018	25.6 ± 1.3	23.2 ± 1.1	20.8 ± 1.0

[a] TTI: time to ignition; PHRR: peak heat release rate; THR: total heat release at 500 s; FPI: fire performance index, FPI = TTI/PHRR; FGR: fire growth rate, FGR = PHRR/T_{PHRR} (T_{PHRR}: time to PHRR); PSPR: peak smoke production rate; TSP: total smoke production at 500 s; AEHC: average effective heat of combustion; and RW: residual weight at 500 s.

DGEBA react with the —NH— groups in PB, leading to inadequate epoxy groups to participate in the crosslinking reaction with DDM, which reduces the crosslinking density and thus T_g value. Meanwhile, the introduction of rigid benzene-rich structure is responsible for the increased *E'* values and thus the rigidity of EP/DDM/PB samples. Similar phenomenon has been reported in previous works about oligomeric-flame-retardant-containing EPs [22,23].

Fig. 3c, d and Table 2 display the tensile strengths, Young's moduli, elongations at break and impact strengths of EP thermosets. The neat EP/DDM sample shows an intrinsically brittle fracture nature, with a tensile strength of 53.37 MPa, a Young's modulus of 1280.2 MPa, an elongation at break of 5.71% and an impact strength of 8.68 kJ/m^2. With the introduction of PB, EP/DDM/PB samples exhibit enhanced mechanical properties. For instance, the elongation at break and impact strength of EP/DDM/PB-3 sample are respectively increased to 7.86% and 13.04 kJ/m^2 (by ~37.7% and ~50.2%), demonstrating the enhanced toughness. Additionally, 5 wt% PB enables EP/DDM/PB-5 sample to achieve a tensile strength of 80.42 MPa and a Young's modulus of 1563.4 MPa, which are 50.7% and 22.1% higher than those of EP/DDM sample, further confirming the improvement in mechanical rigidity and robustness. Such results manifest the reinforcing and toughening effects of PB towards EP thermoset. Notably, unlike the oligomeric PB, both low molecular flame retardants (DA and PD) deteriorate the mechanical properties of EP/DDM/DA-3 and EP/DDM/PD-3 thermosets, which indicates that the oligomeric flame retardants are more suitable for the practical applications relative to the low molecular ones.

To investigate the toughening effect of PB, the microtopographies of Izod impact fractured surfaces for EP/DDM, EP/DDM/PB-3 and EP/DDM/PB-5 samples are studied by SEM, with the micrographs presented in Fig. 4. The fractured surface of pure EP/DDM sample is relatively smooth with some linear cracks, indicating typical brittle fracture characteristic. With the introduction of PB, the fractured surfaces of EP/DDM/PB-3 and EP/DDM/PB-5 samples become rugged, and some small crinkles appear, demonstrating the increased fracture propagation path and area, leading to energy dissipation and thus enhanced toughness [43,44]. Clearly, the flexible B-O bond in PB features higher bond energy than the chemical bonds in EP matrix [45], which contributes to the toughening modification of EP thermoset. In addition, the polar phenylphosphonic group in PB strengthens the interaction between EP matrix and PB, also playing a positive role in toughening EP thermoset [8,46]. Generally, the well-designed oligomeric PB is capable of simultaneously endowing epoxy thermoset with improved mechanical rigidity, robustness and toughness.

3.4. Transparency of EP thermosets

The influence of PB on the optical performances of EP/DDM thermoset is investigated by transmittance/haze tester, UV–Vis spectrophotometer and digital camera, with the results shown in Figs. 5 and S3a. As shown in Fig. 5a and S3a, the neat EP/DDM film exhibits a high transmittance of 84.2% and a low haze of 14.1%, while introducing PB results in the reduced transmittance and increased haze, implying its negative effect on optical performances of epoxy thermoset. Fortunately, the transmittances of EP/DDM/PB films maintain at relatively high levels (66.8–81.3%), and the same downtrend can also be observed in

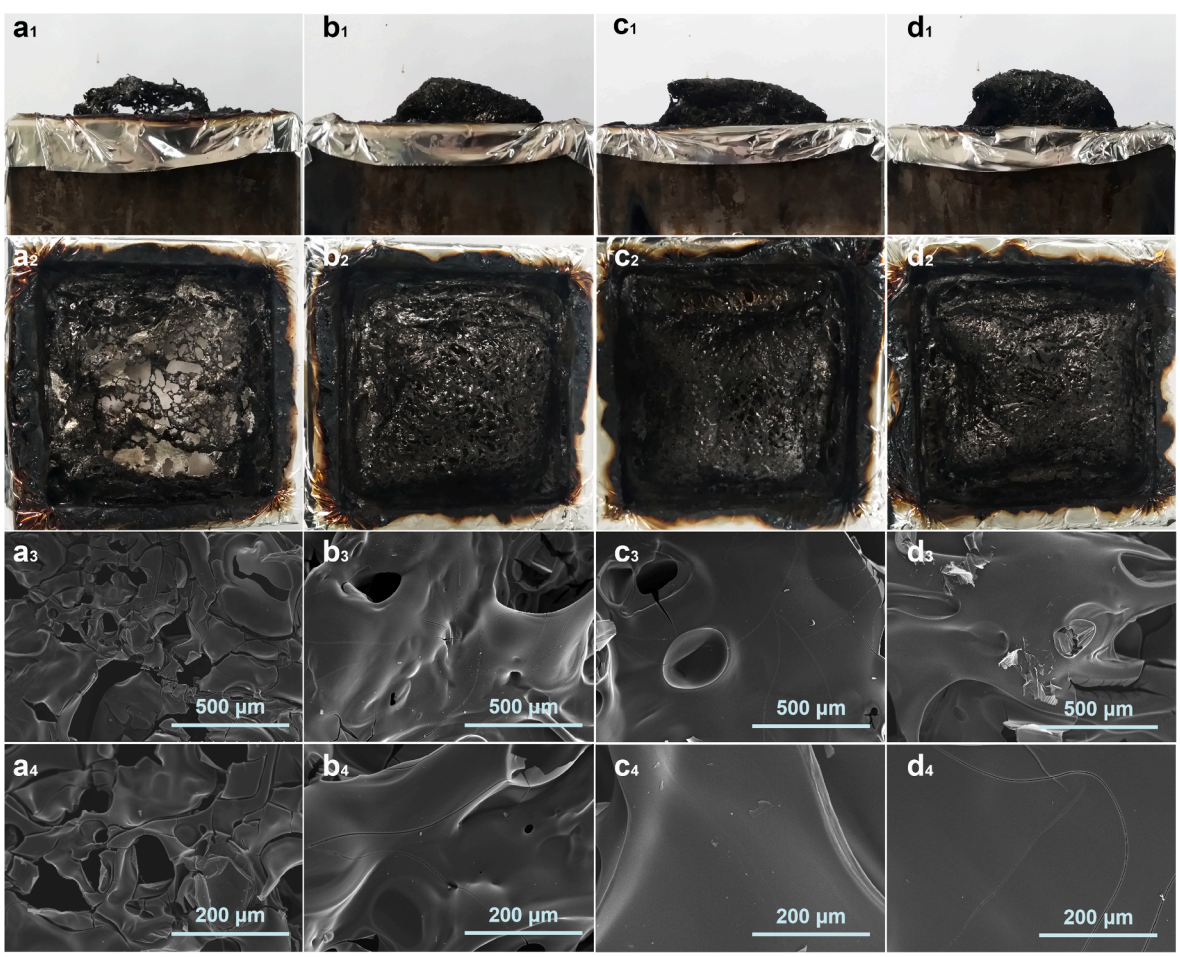

Fig. 7. Digital photos (Top- and side-view) and SEM images of char residues for (a_1-a_4) EP/DDM, (b_1-b_4) EP/DDM/PB-1, (c_1-c_4) EP/DDM/PB-3 and (d_1-d_4) EP/DDM/PB-5 after cone calorimeter tests.

the UV–Vis spectra curves of EP samples in visible region (see Fig. 5b). In addition, from the digital photos (see Fig. 5c–g), we can find that the school emblem of NingboTech University is clearly visible although it is covered by the EP films. However, the EP/DDM/PB films have yellowed as the PB content increases. All these results verify that although PB reduces the transparency of EP samples, the transparency of EP/DDM/PB samples can remain at a relatively high level, which is expected to find applications in the industrial fields where high transparency is required.

The optical performance of epoxy thermoset is mainly determined by the inner crystallization [47,48], and thus the XRD measurement is conducted, with the spectra presented in Fig. S3b. Obviously, the high transmittance of EP/DDM sample is attributed to its non-crystallization characteristic, as reflected by a broad diffraction peak within 2θ = 10°–40°. It is worth noting that all EP/DDM/PB samples also exhibit such broad diffraction peak, which indicates that the addition of PB do not affect the amorphous feature of epoxy thermoset. Thus, the addition of PB can maintain the high transparency of EP/DDM/PB samples.

3.5. Flame retardancy and smoke suppression of EP thermosets

The LOI and UL-94 testes are conducted to initially evaluate the flame retardancy of EP thermosets, with the results shown in Fig. 6a. Typically, pure EP/DDM sample suffers from high inflammability, which shows a low LOI of 26.5% and cannot pass the UL-94 test, indicating the significance of flame retardancy modification. Unfortunately,

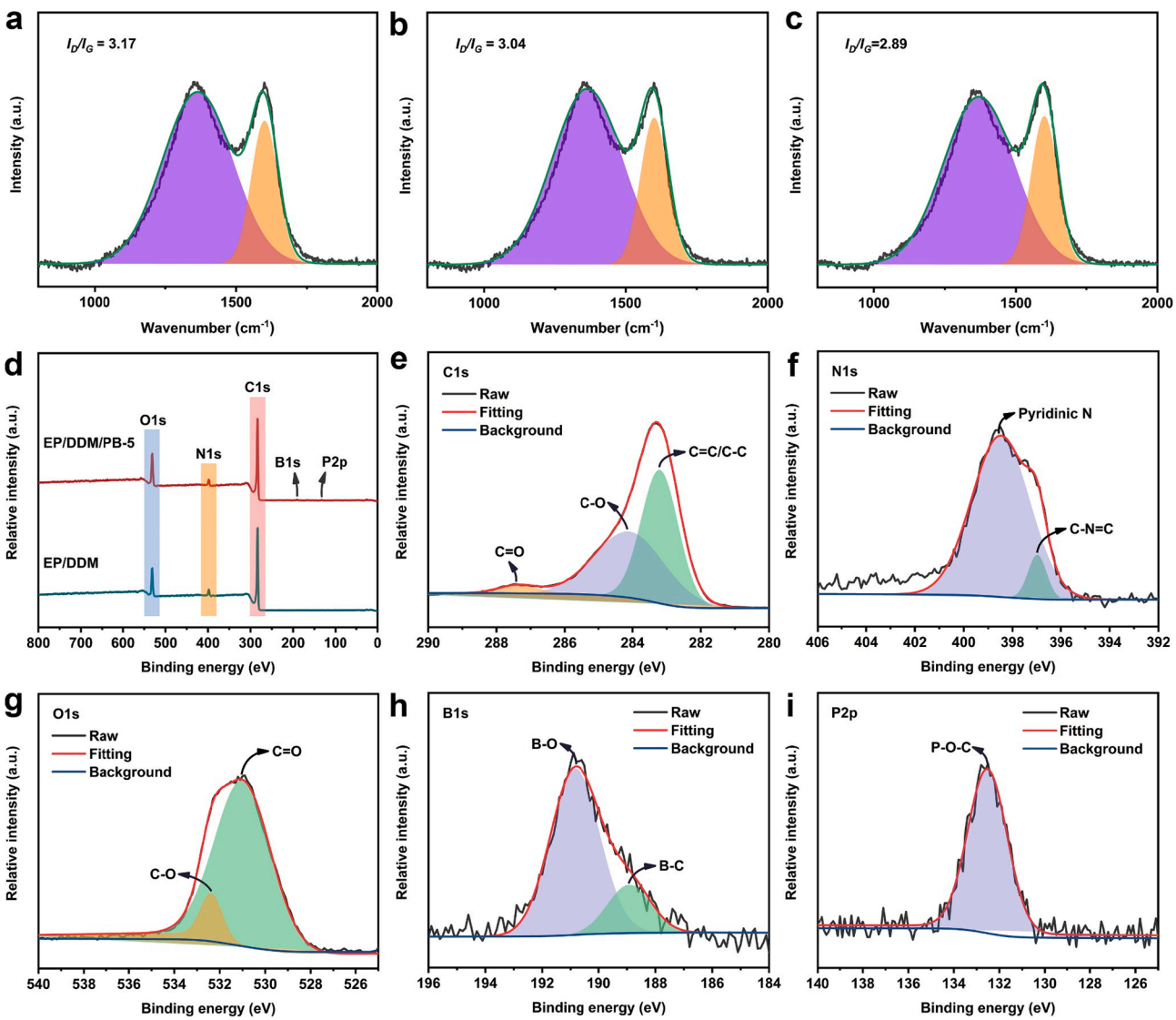

Fig. 8. Raman spectra of residual chars for (a) EP/DDM, (b) EP/DDM/PB-3 and (c) EP/DDM/PB-5 samples, (d) XPS spectra of residual chars for EP/DDM and EP/DDM/PB-5 samples, (e) C1s, (f) N1s, (g) O1s, (h) B1s and (i) P2p high-resolution XPS spectra of chars for EP/DDM/PB-5 sample.

Table 4
XPS parameters of char residues for EP/DDM and EP/DDM/PB-5 samples.

Sample	Atomic ratio (%)					Area (%)			C_{ox}/C_a ratio[a]
	C1s	N1s	O1s	P2p	B1s	C1s (C═C/C-C)	C1s (C—O)	C1s (C═O)	
EP/DDM	83.11	4.61	12.28	/	/	44.5	51.6	3.8	1.24
EP/DDM/PB-5	78.85	4.95	13.92	0.44	1.84	49.8	46.8	3.4	1.01

[a] C_{ox}: oxidized carbons (C_{ox} = total area of C—O and C═O peaks), and C_a: aliphatic and aromatic carbons (C_a = area of C═C and C—C peaks).

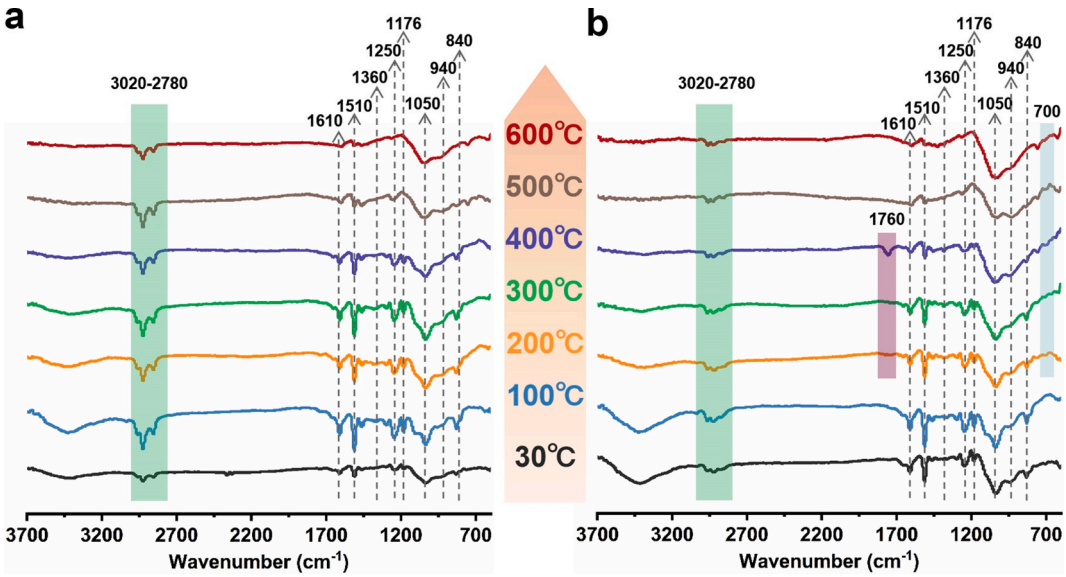

Fig. 9. RT-FTIR spectra of (a) EP/DDM and (b) EP/DDM/PB-5 samples at different temperatures in air condition.

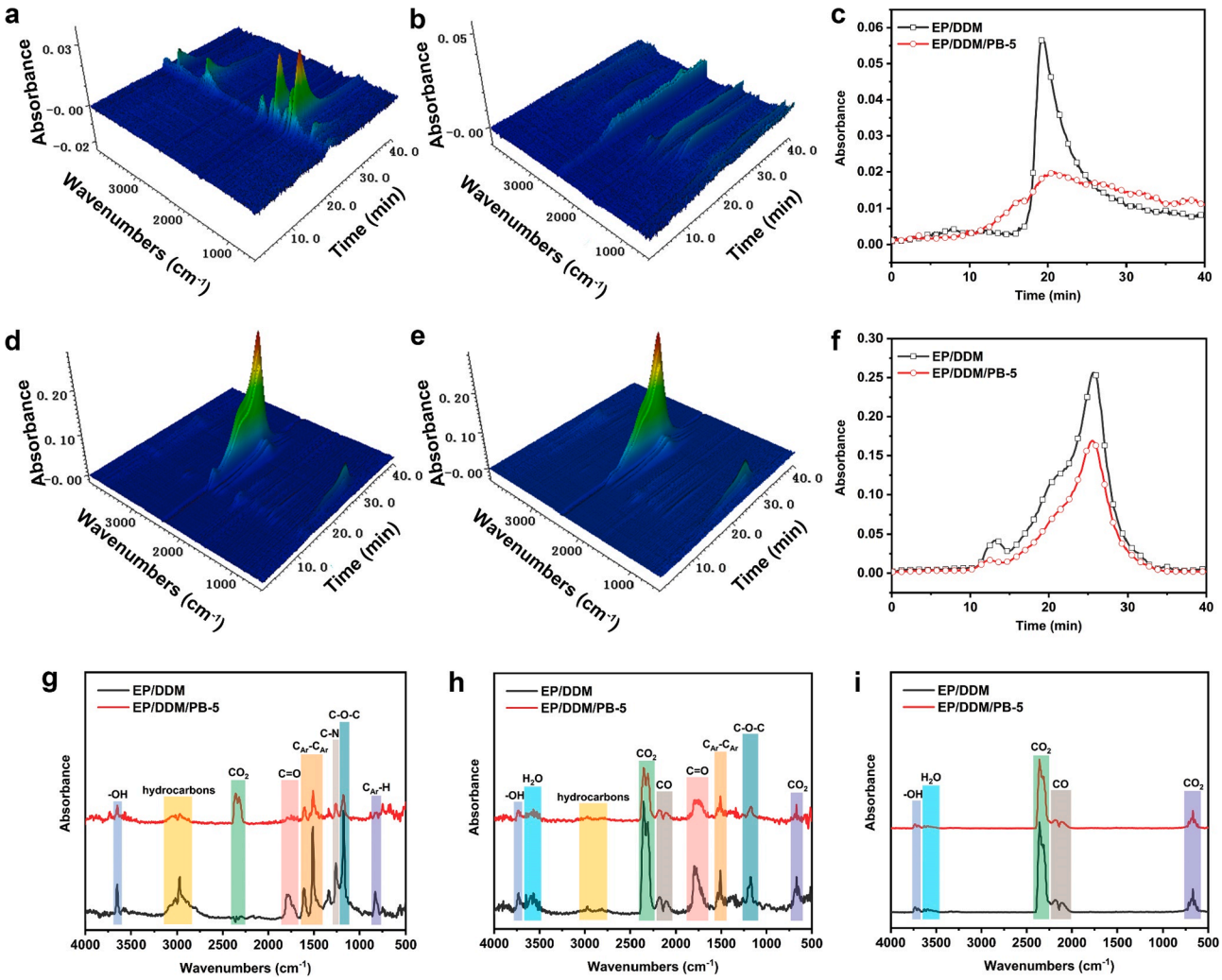

Fig. 10. 3D TG-IR spectra of (a) EP/DDM and (b) EP/DDM/PB-5 samples in N_2 condition, (c) absorbance intensity *vs* time curves of EP/DDM and EP/DDM/PB-5 samples in N_2 condition, 3D TG-IR spectra of (d) EP/DDM and (e) EP/DDM/PB-5 samples under air flow, (f) absorbance intensity *vs* time curves of EP/DDM and EP/DDM/PB-5 samples under air flow, and FTIR spectra of EP/DDM and EP/DDM/PB-5 samples at (g) T_{max1} in N_2 condition, (h) T_{max1} and (i) T_{max2} in air condition.

Table 5
Supposed pyrolytic products of EP/DDM sample determined by MS.

Peak	Retention time (min)	*m/z*	Assigned structure
1	4.5	207	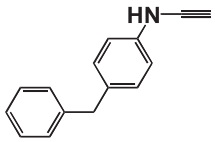
2	6.9	94	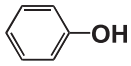
3	7.2	282	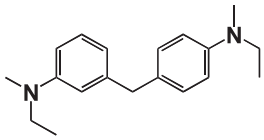
4	7.8	136	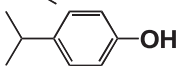
5	8.9	116	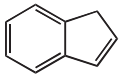
6	10.5	114	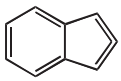
7	12.6	174	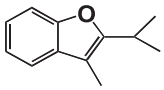
8	14.1	119	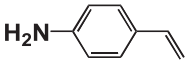
9	15.1	200	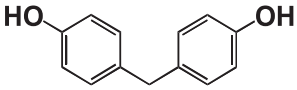
10	16.2	172	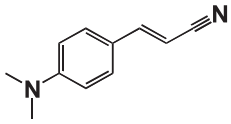
11	17.4	228	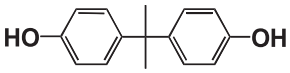
12	18.4	242	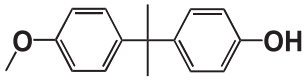
13	19.4	256	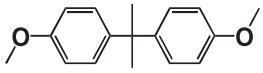
14	21.3	284	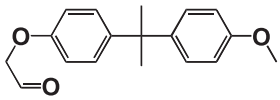
15	23.1	340	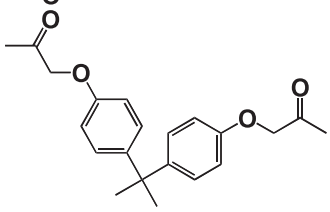
16	24.1	429	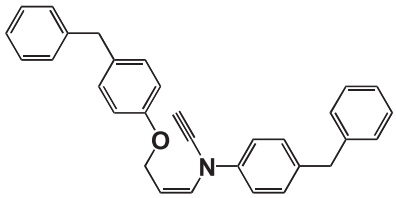

Table 5 (*continued*)

Peak	Retention time (min)	*m/z*	Assigned structure
17	24.6	405	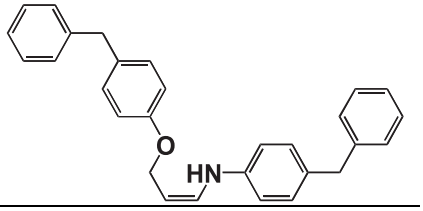

the incorporation of DA or PD only slightly elevates the LOIs and UL-94 ratings of EP/DDM/DA-3 and EP/DDM/PD-3, e.g., the LOIs increasing to 28.1% and 28.6%, respectively. By contrast, PB endows EP/DDM/PB samples with satisfied flame retardancy at a low loading level, indicating high flame retardant efficiency. For instance, 3 wt% of PB enables EP/DDM/PB-3 sample to achieve a UL-94 V-0 rating, and 5 wt% of PB increases the LOI of EP/DDM/PB-5 sample to 35.6%. Obviously, under the same content (3 wt%), PB exhibits higher efficiency than DA and PD, verifying the synergistic flame retardant effect of B, N and P elements in PB.

Cone calorimeter tests, capable of simulating a real fire [49–51], are performed to further investigate the flame retardant and smoke suppressive performances of EP samples, with the curves and data shown in Fig. 6 and Table 3. During this test, EP/DDM sample is ignited at 62 s and then burns rapidly and fiercely, with the highest PHRR and THR of 1311 kW/m^2 and 87.5 MJ/m^2 among all as-fabricated EP samples (see Table 3). With the introduction of PB, the TTIs of EP/DDM/PB samples are prolonged, because PB enhances the thermo-oxidative stability of EP matrix, which is confirmed by the TGA results in air condition. Additionally, EP/DDM/PB samples exhibit significantly reduced PHRR and THR values (see Fig. 6b and c). For example, the PHRR and THR of EP/DDM/PB-3 sample are reduced to 989 kW/m^2 and 76.7 MJ/m^2 by ~24.6% and ~12.3%, and those of EP/DDM/PB-5 sample are decreased to 923 kW/m^2 and 78.2 MJ/m^2 by ~29.6% and ~10.6%. Such results further confirm the significant role of PB in flame retardancy modification of EP thermoset. The synergism of B, N and P elements can also be found when comparing the PHRR and THR between EP/DDM/PB-3, EP/DDM/DA-3 and EP/DDM/PD-3 samples. The FPI and FGR that are able to evaluate the fire safety of materials [52] are calculated and listed in Table 3. Higher FPI and lower FGR demonstrate higher fire safety of materials [53]. Obviously, EP/DDM/PB samples are featured by higher FPI and lower FGR relative to EP/DDM, EP/DDM/DA-3 and EP/DDM/PD-3 samples, further manifesting higher fire safety. Thus, PB significantly improves the fire safety of EP/DDM thermoset at a low addition because of the combination of boron, nitrogen and phosphorus.

In addition to flame retardancy, the smoke suppression of EP samples is also studied thoroughly, with the SPR and TSP curves shown in Fig. 6e and f. Clearly, pure EP/DDM sample releases abundant smoke during combustion because of its high inflammability, of which the PSPR and TSP reach 0.453 m^2/s and 35.4 m^2, respectively (see Table 3). Both DA and PD cannot inhibit the smoke release of EP samples, while PB exhibits obvious smoke suppressive function. For instance, the PSPR and TSP of EP/DDM/PB-5 sample are decreased to 0.286 m^2/s and 25.6 m^2, which are 36.9% and 27.7% lower than those of EP/DDM sample. Meanwhile, EP/DDM/PB samples show remarkably increased RWs, which are 27.1–101.9% higher than that of EP/DDM sample. Such change in RW manifests that the combustible fragments released into fire zone is significantly reduced, thus leading to the enhanced smoke-suppressive performances. According to previous works, AEHC is a specific parameter to evaluate the combustion degree of gaseous-phase fragments and thus the flame retardant mechanism in gas phase [54,55]. Therefore, the AEHCs of EP samples are listed and compared in Table 3. Compared with EP/DDM sample, EP/DDM/PB samples only show slight reductions in

AEHC, which demonstrates the limited flame-retardant function of PB in gaseous phase. In general, PB inhibits the heat transfer and smoke generation *via* its condensed-phase effect in promoting the formation of carbonaceous protective layer during combustion.

3.6. Condensed phase

To analyze the condensed-phase mechanism, the macro- and micro-morphologies of char layers for EP/DDM and EP/DDM/PB samples after cone calorimeter tests are investigated by digital camera and SEM, with the photographs presented in Fig. 7. As shown in Fig. 7a1 and a2, pure EP/DDM sample is almost burned out after test, and just leaves a fragile and broken char layer. Meanwhile, there are many holes and cracks on the char surface, leading to unacceptable flame retardancy (see Fig. 7a3 and a4). With the introduction of PB, the morphologies of char layers for EP/DDM/PB samples have been significantly improved, which become intumescent and intact. Meanwhile, the char surfaces of EP/DDM/PB samples are continuous and compact (see Fig. 7b3–d3 and b4–d4), which are conducive to protecting the underlying matrix during combustion. Supposedly, the P- and B-containing compounds generated by PB promote the formation of a dense and continuous char from epoxy matrix during combustion, and the N-based fragments derived from PB make the char swollen [56,57]. Thus, the formation of such dense and intumescent char layers is attributed to the synergy of B, N and P in condensed phase and contributes to retarding the heat transfer, smoke release and protecting the underlying matrix, thus enhancing the flame retardancy and smoke suppression of EP thermosets.

In addition, the chemical constitutions of residual chars for EP/DDM and EP/DDM/PB samples after cone calorimeter tests are studied by Raman spectroscopy and XPS technique, with the spectra shown in Fig. 8. As shown in Fig. 8a–c, all Raman spectra show D and G bands, which are respectively located at 1350 and 1600 cm^{-1} and assigned to the disordered-carbon and graphitic-carbon vibrations [58,59]. The integral area ratio of D and G bands (I_D/I_G) manifests the graphitization degree and thermal stability of char residue, and the lower I_D/I_G, the higher graphitization degree and thermal stability [60]. The I_D/I_G value of EP/DDM char is the highest among all chars, and those of EP/DDM/PB chars are gradually reduced with the increasing content of PB. Hence, the introduction of PB increases the graphitization degree and thermal stability of char layer, thus leading to the enhanced flame retardancy and smoke suppression.

Fig. 8d–i and S4 display the XPS spectra of char layers for EP/DDM and EP/DDM/PB-5 samples, with the data listed in Table 4. As presented in Fig. 8d and Table 4, both EP/DDM and EP/DDM/PB-5 chars show abundant carbon, oxygen and nitrogen atoms, but boron and phosphorus atoms appear in the char of EP/DDM/PB-5 sample. Obviously, major P and B atoms are remained in char layer to exert condensed-phase flame-retardant effect during combustion. As shown in Figs. S4a and 8e, the C1s spectra of EP/DDM and EP/DDM/PB-5 chars are fitted to three deconvoluted peaks (C═C/C—C, C—O and C═O peaks at 283.2, 284.2 and 287.5 eV) [61]. For both N1s spectra (see Figs. S4b and 8f), there are two deconvoluted peaks at 397.0 and 398.5 eV, belonging to pyridinic N and C—N═C, respectively [62]. In terms of O1s spectra (see Figs. S4c and 8g), two deconvoluted peaks appear at 531.0 and 532.4 eV, which are assigned to C═O and C—O, respectively [63]. In addition, the char of EP/DDM/PB-5 sample exhibits two deconvoluted peaks of B—O and B—C at 190.8 and 188.9 eV [64] in Fig. 8h, and it shows one peak of P—O—C at 132.5 eV [65] in Fig. 8i. Such results indicate that abundant B atoms function in condensed phase *via* forming thermally-stable oxides and crosslinking with polyaromatic structures. Meanwhile, the P atoms also participate in the crosslinking of char residue during combustion. Hence, both B and P atoms of PB mainly exert flame-retardant effect in condensed phase *via* involving in the crosslinked reaction of char layer and forming thermally-stable oxides. Besides, as shown in Table 4, the char of EP/DDM/PB-5 sample exhibits lower C_{ox}/C_a ratio than that of EP/DDM sample, further verifying the improved

Table 6
Supposed pyrolytic products of EP/DDM/PB-5 sample determined by MS.

Peak	Retention time (min)	*m/z*	Assigned structure
1	4.5	207	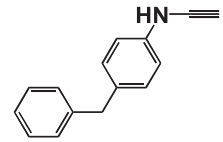
2	6.9	94	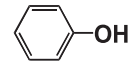
3	7.8	136	
4	8.9	93	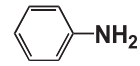
5	10.3	134	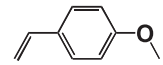
6	11.8	134	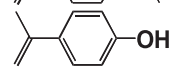
7	13.9	176	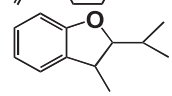
8	15.1	156	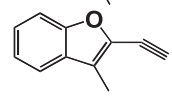
9	15.7	242	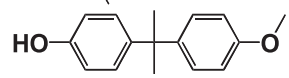
10	16.2	172	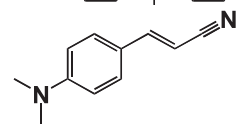
11	17.4	228	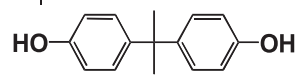
12	18.4	222	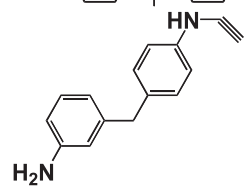
13	19.4	256	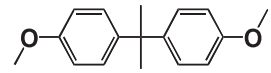
14	21.3	284	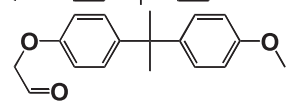
15	23.1	340	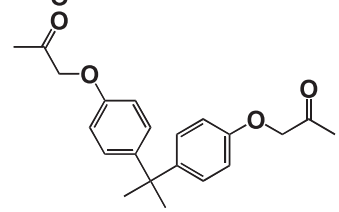
16	24.6	429	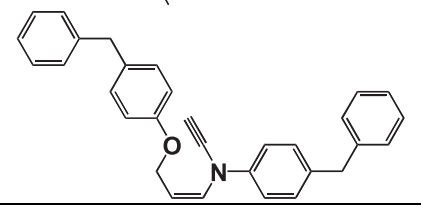

thermal oxidative resistance of char residue due to the addition of PB [66,67].

The RT-FTIR analyses of EP/DDM and EP/DDM/PB-5 samples in air conditions are conducted to further study the influence of PB on the thermal oxidation evolution of EP samples, with the spectra in different decomposition temperatures shown in Fig. 9. The characteristic absorption peaks of EP matrix can be observed at 3020–2780 cm^{-1} (hydrocarbons), 1610 and 1510 cm^{-1} (aromatic compounds), 1360 cm^{-1} (O—H), 1250 cm^{-1} (C—N), 1176 cm^{-1} (aliphatic ethers), 1050 cm^{-1} (=C—H), 940 cm^{-1} (tri-substituted aromatic compounds) and 840 cm^{-1} (C—H) in both RT-FTIR spectra [68,69]. Obviously, the peak of O—H first disappears during thermal oxidation procedure, which is mainly due to the dehydration and dehydrogenation of the secondary alcoholic groups in EP chains [41]. Additionally, due to the weak C—O and C—N bonds, the peak of aliphatic ethers disappears at 500 °C, and that of C—N vanishes at 600 °C in both RT-FTIR spectra. All these results indicate that the thermal oxidation degradation of EP/DDM thermosets originates with the breakage of O—H, C—O and C—N bonds in the skeleton. At 600 °C, only characteristic peaks belonging to aromatic structures (1610, 1510, 1050 and 940 cm^{-1}) can be observed, demonstrating that the char residues are mainly composed of polyaromatic compounds. Notably, the peaks of polyaromatic structures for EP/DDM/PB-5 sample are more obvious than those for EP/DDM sample in 400–600 °C, further indicating the condensed-phase flame-retardant function of PB. Unlike EP/DDM sample, the EP/DDM/PB-5 sample exhibits the absorption peak of C=O at 1760 cm^{-1} in 200–400 °C, demonstrating the improved oxidation resistance due to the incorporation of PB [55,70]. In addition, the peaks of RT-FTIR spectra for EP/DDM/PB-5 sample at 700 cm^{-1} in 200–600 °C are assigned to B—O—B structure, verifying the formation of boron oxide during thermal oxidation evolution [71]. Thus, the RT-FTIR results validate that PB functions in condensed phase to enhance thermal oxidation resistance of char layer and thus fire safety of EP thermoset *via* promoting the formation of polyaromatic structures and generating thermally-stable oxides.

3.7. Gaseous phase

The TG-IR analyses of EP/DDM and EP/DDM/PB-5 samples in N_2 or air condition are performed to investigate the gaseous-phase mechanism, with the spectra presented in Fig. 10. In both nitrogen and air conditions, EP/DDM/PB-5 thermoset show significantly reduced peak intensities of gaseous products compared with EP/DDM thermoset (see Fig. 10a–f). As shown in Fig. 10g–i, the gaseous decomposition products of both EP/DDM and EP/DDM/PB-5 thermosets mainly involve H_2O (O—H, 3650 cm^{-1}), hydrocarbons (2840–3150 cm^{-1}), CO_2 (2260–2410 cm^{-1}), CO (2010–2230 cm^{-1}), carbonyl compounds (1780 cm^{-1}), aromatic compounds (1400–1650, 830 cm^{-1}), C—N-containing compounds (1260 cm^{-1}) and aliphatic ethers (1170 cm^{-1}). Notably, similar downtrend can also be observed when comparing the peak intensities of gaseous products for EP/DDM and EP/EP/DDM/PB-5 samples at T_{max}s. As mentioned in *Section 3.6*, PB facilitates the formation of polyaromatic structures during the thermal decomposition of EP matrix, resulting in more chars remained in condensed phase and less fragments released in gaseous phase. Based on these results, it is speculated that more protective shields are generated and less combustible fragments (fuels) are released into fire zone during combustion of EP/DDM/PB-5 sample, which is responsible for the enhancements in flame retardancy and smoke suppression.

Py-GC/MS analyses of EP/DDM and EP/DDM/PB-5 samples are conducted to gain more information about the pyrolysis behaviors, with the GC chromatograms and the supposed pyrolysis fragments determined by MS presented in Fig. S5 and Tables 5 and 6. In comparison to EP/DDM sample, the GC chromatogram of EP/DDM/PB-5 sample shows reduced peak intensities (see Fig. S5), also indicating the suppression effect of PB in the release of pyrolysis fragments. Meanwhile, the pyrolytic products of EP/DDM/PB-5 sample are similar to those of EP/DDM sample, and both of them contain abundant aniline- and phenol-derived fragments, demonstrating the breakage of C-N and C-O bonds in EP chains at initial pyrolysis stage (see Tables 5 and 6). Such phenomenon is well consistent with the RT-FTIR results. When the retention time of EP/DDM/PB-5 sample is above 19 min, the pyrolysis fragments with larger molecular weights (m/z = 256, 284, 340, 429 and 405) are obviously reduced and even disappear, meaning that most of them are remained in condensed phase to form polyaromatic compounds during pyrolysis procedure.

In sum, during combustion, both P- and B-containing compounds generated by PB facilitate the cross-linking of char layer and form thermally-stable oxides in condensed phase, and meanwhile N-based noncombustible gases derived from PB make the char layer become intumescent. Therefore, such intumescent and dense char decreases the transfer of heat between fire and matrix, and suppresses the release of combustible fragments and smoke, bringing about obvious enhancements in flame retardancy and smoke suppression.

4. Conclusions

In this work, a novel multifunctional highly efficient boron-containing polyphosphonamide (PB) is successfully synthesized and used to fabricate high-performance EPs (EP/DDM/PBs). Notably, only 3 wt% of PB endows EP with a high LOI of 32.2%, a UL-94 V-0 classification and a ~32.2% decrease in PSPR. The high flame-retardant and smoke-suppressive efficiency is attributed the synergy of P, B and N atoms in PB, which makes it superior to the previously-reported counterparts. In addition, PB exhibits reinforcing and toughening effects towards EP, 3 wt% of which increases the tensile strength, elongation at break and impact strength by ~29.8%, ~37.7% and ~50.2%, respectively. The as-prepared EP thermoset remains high glass transition temperature (180 °C) and transmittance (76.3%). This work provides a rational methodology for creating high-efficiency polyphosphonamides with manifold functions to fabricate mechanically strong/tough, thermally-resistant, transparent, flame-retardant and smoke-suppressive EPs, which are expected to drive the development of oligomeric/polymeric flame retardants in the future.

Declaration of Competing Interest

The authors declare that they have no known competing financial interests or personal relationships that could have appeared to influence the work reported in this paper.

Acknowledgements

This work was supported by the National Natural Science Foundation of China (No. 51991355 & 51903193), the Non-profit Project of Science and Technology Department of Ningbo (No. 2019C50029) and Public Technical Application Project of Zhejiang in Industry (No. LGG21E030004).

Appendix A. Supplementary data

Supplementary data to this article can be found online at https://doi.org/10.1016/j.cej.2021.131578.

References

[1] G. Li, P. Zhang, S. Huo, Y. Fu, L. Chen, Y. Wu, Y. Zhang, M. Chen, X. Zhao, P. Song, Mechanically strong, thermally healable, and recyclable epoxy vitrimers enabled by ZnAl-layer double hydroxides, ACS Sustain. Chem. Eng. 9 (6) (2021) 2580–2590.

[2] Y. Zhang, P. Song, S. Fu, F. Chen, Morphological structure and mechanical properties of epoxy/polysulfone/cellulose nanofiber ternary nanocomposites, Compos. Sci. Technol. 115 (2015) 66–71.

[3] H. Yang, B. Shi, Y. Xue, Z. Ma, L. Liu, L. Liu, Y. Yu, Z. Zhang, P.K. Annamalai, P. Song, Molecularly engineered lignin-derived additives enable fire-retardant, UV-shielding, and mechanically strong polylactide biocomposites, Biomacromolecules 22 (4) (2021) 1432–1444.

[4] Y.-F. Ai, F.-Q. Pang, Y.-L. Xu, R.-K. Jian, Multifunctional phosphorus-containing triazolyl amine toward self-intumescent flame-retardant and mechanically strong epoxy resin with high transparency, Ind. Eng. Chem. Res. 59 (26) (2020) 11918–11929.

[5] R.-K. Jian, Y.-F. Ai, L. Xia, L.-J. Zhao, H.-B. Zhao, Single component phosphamide-based intumescent flame retardant with potential reactivity towards low flammability and smoke epoxy resins, J. Hazard. Mater. 371 (2019) 529–539.

[6] Y. Qiu, L. Qian, H. Feng, S. Jin, J. Hao, Toughening effect and flame-retardant behaviors of phosphaphenanthrene/phenylsiloxane bigroup macromolecules in epoxy thermoset, Macromolecules 51 (23) (2018) 9992–10002.

[7] L. Xu, Z. Fang, P. Song, M. Peng, Functionalization of carbon nanotubes by corona-discharge induced graft polymerization for the reinforcement of epoxy nanocomposites, Plasma Process. Polym. 7 (9-10) (2010) 785–793.

[8] Y. Qiu, L. Qian, Y. Chen, J. Hao, Improving the fracture toughness and flame retardant properties of epoxy thermosets by phosphaphenanthrene/siloxane cluster-like molecules with multiple reactive groups, Compos. B Eng. 178 (2019), 107481.

[9] W. Xie, S. Huang, D. Tang, S. Liu, J. Zhao, Biomass-derived Schiff base compound enabled fire-safe epoxy thermoset with excellent mechanical properties and high glass transition temperature, Chem. Eng. J. 394 (2020), 123667.

[10] S.M. Seraji, H. Gan, S. Issazadeh, R.J. Varley, Investigation of the dual polymerization of rapid curing organophosphorous modified epoxy/amine resins and subsequent flame retardancy, Macromol. Chem. Phys. 222 (7) (2021) 2000342, https://doi.org/10.1002/macp.v222.710.1002/macp.202000342.

[11] J.C. Markwart, A. Battig, L. Zimmermann, M. Wagner, J. Fischer, B. Schartel, F. R. Wurm, Systematically controlled decomposition mechanism in phosphorus flame retardants by precise molecular architecture: P-O vs P–N, ACS Appl. Polym. Mater. 1 (5) (2019) 1118–1128.

[12] Y. Fang, J. Miao, X. Yang, Y. Zhu, G. Wang, Fabrication of polyphosphazene covalent triazine polymer with excellent flame retardancy and smoke suppression for epoxy resin, Chem. Eng. J. 385 (2020), 123830.

[13] F. Fang, P. Song, S. Ran, Z. Guo, H. Wang, Z. Fang, A facile way to prepare phosphorus-nitrogen-functionalized graphene oxide for enhancing the flame retardancy of epoxy resin, Compos. Commun. 10 (2018) 97–102.

[14] G. Huang, W. Chen, T. Wu, H. Guo, C. Fu, Y. Xue, K. Wang, P. Song, Multifunctional graphene-based nano-additives toward high-performance polymer nanocomposites with enhanced mechanical, thermal, flame retardancy and smoke suppressive properties, Chem. Eng. J. 410 (2021), 127590.

[15] B. Wang, Y.-J. Xu, P. Li, F.-Q. Zhang, Y. Liu, P. Zhu, Flame-retardant polyester/cotton blend with phosphorus/nitrogen/silicon-containing nano-coating by layer-by-layer assembly, Appl. Surf. Sci. 509 (2020), 145323.

[16] M.M. Velencoso, A. Battig, J.C. Markwart, B. Schartel, F.R. Wurm, Molecular firefighting-how modern phosphorus chemistry can help solve the challenge of flame retardancy, Angew. Chem. Int. Ed. Engl. 57 (33) (2018) 10450–10467.

[17] Y.-Q. Shi, T. Fu, Y.-J. Xu, D.-F. Li, X.-L. Wang, Y.-Z. Wang, Novel phosphorus-containing halogen-free ionic liquid toward fire safety epoxy resin with well-balanced comprehensive performance, Chem. Eng. J. 354 (2018) 208–219.

[18] A. Battig, J.C. Markwart, F.R. Wurm, B. Schartel, Hyperbranched phosphorus flame retardants: multifunctional additives for epoxy resins, Polym. Chem. 10 (31) (2019) 4346–4358.

[19] S. Huo, S. Yang, J. Wang, J. Cheng, Q. Zhang, Y. Hu, G. Ding, Q. Zhang, P. Song, A liquid phosphorus-containing imidazole derivative as flame-retardant curing agent for epoxy resin with enhanced thermal latency, mechanical, and flame-retardant performances, J. Hazard. Mater. 386 (2020), 121984.

[20] Y. Zhang, J. Jing, T. Liu, L. Xi, T. Sai, S. Ran, Z. Fang, S. Huo, P. Song, A molecularly engineered bioderived polyphosphate for enhanced flame retardant, UV-blocking and mechanical properties of poly(lactic acid), Chem. Eng. J. 411 (2021), 128493.

[21] X.-F. Liu, B.-W. Liu, X. Luo, D.-M. Guo, H.-Y. Zhong, L. Chen, Y.-Z. Wang, A novel phosphorus-containing semi-aromatic polyester toward flame retardancy and enhanced mechanical properties of epoxy resin, Chem. Eng. J. 380 (2020), 122471.

[22] Z.-M. Zhu, L.-X. Wang, L.-P. Dong, Influence of a novel P/N-containing oligomer on flame retardancy and thermal degradation of intumescent flame-retardant epoxy resin, Polym. Degrad. Stab. 162 (2019) 129–137.

[23] P. Wang, F. Yang, L. Li, Z. Cai, Flame retardancy and mechanical properties of epoxy thermosets modified with a novel DOPO-based oligomer, Polym. Degrad. Stab. 129 (2016) 156–167.

[24] X. Wang, Y. Hu, L. Song, H. Yang, W. Xing, H. Lu, Synthesis and characterization of a DOPO-substitued organophosphorus oligomer and its application in flame retardant epoxy resins, Prog. Org. Coat. 71 (1) (2011) 72–82.

[25] J. Zhang, X. Mi, S. Chen, Z. Xu, D. Zhang, M. Miao, J. Wang, A bio-based hyperbranched flame retardant for epoxy resins, Chem. Eng. J. 381 (2020), 122719.

[26] Q. Zhang, S. Yang, J. Wang, J. Cheng, Q. Zhang, G. Ding, Y. Hu, S. Huo, A DOPO based reactive flame retardant constructed by multiple heteroaromatic groups and its application on epoxy resin: curing behavior, thermal degradation and flame retardancy, Polym. Degrad. Stab. 167 (2019) 10–20.

[27] H. Wu, B. Zeng, J. Chen, T. Wu, Y. Li, Y. Liu, L. Dai, An intramolecular hybrid of metal polyhedral oligomeric silsesquioxanes with special titanium-embedded cage structure and flame retardant functionality, Chem. Eng. J. 374 (2019) 1304–1316.

[28] H. Gan, S.M. Seraji, J. Zhang, S.R. Swan, S. Issazadeh, R.J. Varley, Synthesis of a phosphorus-silicone modifier imparting excellent flame retardancy and improved mechanical properties to a rapid cure epoxy, React. Funct. Polym. 157 (2020), 104743.

[29] C. Ma, S. Qiu, B. Yu, J. Wang, C. Wang, W. Zeng, Y. Hu, Economical and environment-friendly synthesis of a novel hyperbranched poly (aminomethylphosphine oxide-amine) as co-curing agent for simultaneous improvement of fire safety, glass transition temperature and toughness of epoxy resins, Chem. Eng. J. 322 (2017) 618–631.

[30] Y. Qiu, L. Qian, W. Xi, Flame-retardant effect of a novel phosphaphenanthrene/triazine-trione bi-group compound on an epoxy thermoset and its pyrolysis behaviour, RSC Adv. 6 (61) (2016) 56018–56027.

[31] S. Huo, J. Wang, S. Yang, J. Wang, B. Zhang, B.o. Zhang, X.i. Chen, Y. Tang, Synthesis of a novel phosphorus-nitrogen type flame retardant composed of maleimide, triazine-trione, and phosphaphenanthrene and its flame retardant effect on epoxy resin, Polym. Degrad. Stab. 131 (2016) 106–113.

[32] H. Duan, Y. Chen, S. Ji, R. Hu, H. Ma, A novel phosphorus/nitrogen-containing polycarboxylic acid endowing epoxy resin with excellent flame retardance and mechanical properties, Chem. Eng. J. 375 (2019), 121916.

[33] S. Huo, Z. Liu, J. Wang, Thermal properties and flame retardancy of an intumescent flame-retarded epoxy system containing phosphaphenanthrene, triazine-trione and piperidine, J. Therm. Anal. Calorim. 139 (2) (2020) 1099–1110.

[34] H.J. Duan, J.F. Cao, Y.S. Chen, J.S. Wang, S. Ji, H.R. Ma, A phosphorus/boron-containing triazine-trione derivative endowing epoxy resin with excellent flame retardance, Express Polym. Lett. 14 (10) (2020) 908–923.

[35] W. Xu, W. Li, M. Ren, J. Yin, Synthesis and characterization of flame-retardant polyurethane elastomers using phosphorus-containing chain extender, Asian J. Chem. 25 (10) (2013) 5683–5685.

[36] S.A. Kumar, Z. Denchev, Development and characterization of phosphorus-containing siliconized epoxy resin coatings, Prog. Org. Coat. 66 (1) (2009) 1–7.

[37] B. Schartel, A.I. Balabanovich, U. Braun, U. Knoll, J. Artner, M. Ciesielski, M. Döring, R. Perez, J.K.W. Sandler, V. Altstädt, T. Hoffmann, D. Pospiech, Pyrolysis of epoxy resins and fire behavior of epoxy resin composites flame-retarded with 9,10-dihydro-9-oxa-10-phosphaphenanthrene-10-oxide additives, J. Appl. Polym. Sci. 104 (4) (2007) 2260–2269.

[38] S. Yang, Q. Zhang, Y. Hu, Preparation and investigation of flame-retardant epoxy resin modified with a novel halogen-free flame retardant containing phosphaphenanthrene, triazine-trione, and organoboron units, J. Appl. Polym. Sci. 134 (37) (2017) 45291, https://doi.org/10.1002/app.45291.

[39] J. Feng, X. Xu, Z. Xu, H. Xie, P. Song, L. Li, G. Huang, H. Wang, One-pot, solvent- and catalyst-free synthesis of polyphosphoramide as an eco-benign and effective flame retardant for poly(lactic acid), ACS Sustain. Chem. Eng. 8 (44) (2020) 16612–16623.

[40] J. Wang, B. Yuan, W. Cai, S. Qiu, Q. Tai, H. Yang, Y. Hu, Facile design of transition metal based organophosphorus hybrids towards the flame retardancy reinforcement and toxic effluent elimination of polystyrene, Mater. Chem. Phys. 214 (2018) 209–220.

[41] S. Huo, P. Song, B. Yu, S. Ran, V.S. Chevali, L. Liu, Z. Fang, H. Wang, Phosphorus-containing flame retardant epoxy thermosets: recent advances and future perspectives, Prog. Polym. Sci. 114 (2021) 101366, https://doi.org/10.1016/j.progpolymsci.2021.101366.

[42] W. He, P. Song, B. Yu, Z. Fang, H. Wang, Flame retardant polymeric nanocomposites through the combination of nanomaterials and conventional flame retardants, Prog. Mater. Sci. 114 (2020), 100687.

[43] R.-K. Jian, X.-B. Lin, Z.-Q. Liu, W. Zhang, J. Zhang, L. Zhang, Z. Li, D.-Y. Wang, Rationally designed zinc borate@ ZIF-8 core-shell nanorods for curing epoxy resins along with low flammability and high mechanical property, Compos. B Eng. 200 (2020), 108349.

[44] Z. Xu, P. Song, J. Zhang, Q. Guo, Y.-W. Mai, Epoxy nanocomposites simultaneously strengthened and toughened by hybridization with graphene oxide and block ionomer, Compos. Sci. Technol. 168 (2018) 363–370.

[45] Y.-R. Luo, Comprehensive Handbook of Chemical Bond Energies, CRC Press, 2007.

[46] F. Chu, C. Ma, T. Zhang, Z. Xu, X. Mu, W. Cai, X. Zhou, S. Ma, Y. Zhou, W. Hu, L. Song, Renewable vanillin-based flame retardant toughening agent with ultra-low phosphorus loading for the fabrication of high-performance epoxy thermoset, Compos. B Eng. 190 (2020), 107925.

[47] T. Sai, S. Ran, Z. Guo, H. Yan, Y. Zhang, H. Wang, P. Song, Z. Fang, Transparent, highly thermostable and flame retardant polycarbonate enabled by rod-like phosphorous-containing metal complex aggregates, Chem. Eng. J. 409 (2021), 128223.

[48] Z. Shao, W. Yue, M. Piao, J. Ma, X. Lv, D. Wang, Q.i. Wang, An excellent intrinsic transparent epoxy resin with high flame retardancy: synthesis, characterization, and properties, Macromol. Mater. Eng. 304 (10) (2019) 1900254, https://doi.org/10.1002/mame.v304.1010.1002/mame.201900254.

[49] F. Fang, S. Huo, H. Shen, S. Ran, H. Wang, P. Song, Z. Fang, A bio-based ionic complex with different oxidation states of phosphorus for reducing flammability and smoke release of epoxy resins, Compos. Commun. 17 (2020) 104–108.

[50] S. Yang, S. Huo, J. Wang, B. Zhang, J. Wang, S. Ran, Z. Fang, P. Song, H. Wang, A highly fire-safe and smoke-suppressive single-component epoxy resin with switchable curing temperature and rapid curing rate, Compos. B Eng. 207 (2021), 108601.

[51] Y. Xue, M. Shen, S. Zeng, W. Zhang, L. Hao, L.u. Yang, P. Song, A novel strategy for enhancing the flame resistance, dynamic mechanical and the thermal degradation properties of epoxy nanocomposites, Mater. Res. Express 6 (12) (2019) 125003, https://doi.org/10.1088/2053-1591/ab537f.

[52] S. Huo, S. Yang, J. Wang, J. Cheng, Q. Zhang, Y. Hu, G. Ding, Q. Zhang, P. Song, H. Wang, A liquid phosphaphenanthrene-derived imidazole for improved flame

retardancy and smoke suppression of epoxy resin, ACS Appl. Polym. Mater. 2 (8) (2020) 3566–3575.
[53] T. Sai, S. Ran, Z. Guo, H. Yan, Y. Zhang, P. Song, T. Zhang, H. Wang, Z. Fang, Deposition growth of Zr-based MOFs on cerium phenylphosphonate lamella towards enhanced thermal stability and fire safety of polycarbonate, Compos. B Eng. 197 (2020), 108064.
[54] Z. Fu, H. Wang, X. Zhao, X. Li, X. Gu, Y. Li, Flame-retarding nanoparticles as the compatibilizers for immiscible polymer blends: simultaneously enhanced mechanical performance and flame retardancy, J. Mater. Chem. A 7 (9) (2019) 4903–4912.
[55] S. Huo, J. Wang, S. Yang, B. Zhang, Y. Tang, A phosphorus-containing phenolic derivative and its application in benzoxazine resins: curing behavior, thermal, and flammability properties, J. Appl. Polym. Sci. 133 (19) (2016) 43403.
[56] B. Yu, W. Xing, W. Guo, S. Qiu, X. Wang, S. Lo, Y. Hu, Thermal exfoliation of hexagonal boron nitride for effective enhancements on thermal stability, flame retardancy and smoke suppression of epoxy resin nanocomposites via sol–gel process, J. Mater. Chem. A 4 (19) (2016) 7330–7340.
[57] L. Liu, M. Zhu, Y. Shi, X. Xu, Z. Ma, B. Yu, S. Fu, G. Huang, H. Wang, P. Song, Functionalizing MXene towards highly stretchable, ultratough, fatigue- and fire-resistant polymer nanocomposites, Chem. Eng. J. 424 (2021), 130338.
[58] W. Ma, B.o. Xu, L. Shao, Y. Liu, Y. Chen, L. Qian, Synthesis of (1,4-methylenephenylphosphinic acid) piperazine and its application as a flame retardant in epoxy thermosets, Macromol. Mater. Eng. 304 (12) (2019) 1900419, https://doi.org/10.1002/mame.v304.1210.1002/mame.201900419.
[59] B. Yu, A.C.Y. Yuen, X. Xu, Z.-C. Zhang, W. Yang, H. Lu, B. Fei, G.H. Yeoh, P. Song, H. Wang, Engineering MXene surface with POSS for reducing fire hazards of polystyrene with enhanced thermal stability, J. Hazard. Mater. 401 (2021), 123342.
[60] J. Zhang, Z. Li, L.u. Zhang, Y. Yang, D.-Y. Wang, Green synthesis of biomass phytic acid-functionalized UiO-66-NH2 hierarchical hybrids toward fire safety of epoxy resin, ACS Sustain. Chem. Eng. 8 (2) (2020) 994–1003.
[61] Q. Li, D. Liu, Z. Jia, L. Csetenyi, G. Gadd, Fungal biomineralization of manganese as a novel source of electrochemical materials, Curr. Biol. 26 (7) (2016) 950–955.
[62] Y. Shi, C. Liu, Z. Duan, B. Yu, M. Liu, P. Song, Interface engineering of MXene towards super-tough and strong polymer nanocomposites with high ductility and excellent fire safety, Chem. Eng. J. 399 (2020), 125829.
[63] L. Liu, Y. Xu, Y. Di, M. Xu, Y. Pan, B. Li, Simultaneously enhancing the fire retardancy and crystallization rate of biodegradable polylactic acid with piperazine-1,4-diylbis(diphenylphosphine oxide), Compos. B Eng. 202 (2020), 108407.
[64] X.i. Zhou, X. Gao, M. Liu, C. Wang, F. Chu, A poly(5-indolylboronic acid) based molecular imprint doped with carbon dots for fluorometric determination of glucose, Microchim. Acta 184 (10) (2017) 4175–4181.
[65] M. Zhang, X. Ding, Y. Zhan, Y. Wang, X. Wang, Improving the flame retardancy of poly(lactic acid) using an efficient ternary hybrid flame retardant by dual modification of graphene oxide with phenylphosphinic acid and nano MOFs, J. Hazard. Mater. 384 (2020), 121260.
[66] L. Wang, S. Wu, X. Dong, R. Wang, L. Zhang, J. Wang, J. Zhong, L. Wu, X. Wang, A pre-constructed graphene–ammonium polyphosphate aerogel (GAPPA) for efficiently enhancing the mechanical and fire-safety performances of polymers, J. Mater. Chem. A 6 (10) (2018) 4449–4457.
[67] L. Liu, Z. Wang, Facile synthesis of a novel magnesium amino-tris-(methylenephosphonate)-reduced graphene oxide hybrid and its high performance in mechanical strength, thermal stability, smoke suppression and flame retardancy in phenolic foam, J. Hazard. Mater. 357 (2018) 89–99.
[68] J. Hong, T. Wu, H. Wu, B. Zeng, S. Zeng, T. Chen, X. Wang, Z. Lu, C. Yuan, K. Balaji, D.F.S. Petri, L. Dai, Nanohybrid silver nanoparticles@halloysite nanotubes coated with polyphosphazene for effectively enhancing the fire safety of epoxy resin, Chem. Eng. J. 407 (2021) 127087, https://doi.org/10.1016/j.cej.2020.127087.
[69] Y. Qi, Z. Weng, Y. Kou, L. Song, J. Li, J. Wang, S. Zhang, C. Liu, X. Jian, Synthesize and introduce bio-based aromatic s-triazine in epoxy resin: enabling extremely high thermal stability, mechanical properties, and flame retardancy to achieve high-performance sustainable polymers, Chem. Eng. J. 406 (2021), 126881.
[70] S. Yang, J. Wang, S. Huo, J. Wang, Y. Tang, Synthesis of a phosphorus/nitrogen-containing compound based on maleimide and cyclotriphosphazene and its flame-retardant mechanism on epoxy resin, Polym. Degrad. Stabil. 126 (2016) 9–16.
[71] G. Gao, L. Hu, H. Fan, G. Wang, K. Li, S. Feng, S. Fan, H. Chen, Effect of Bi_2O_3 on physical, optical and structural properties of boron silicon bismuthate glasses, Opt. Mater. 32 (1) (2009) 159–163.